JPL PUBLICATION 77-72

Final Report: Medical Ultrasonic Tomographic System

Prepared for

National Institutes of Health
Division of General Medical Sciences

by

Jet Propulsion Laboratory
California Institute of Technology
Pasadena, California 91103

JET PROPULSION LABORATORY *California Institute of Technology • 4800 Oak Grove Drive, Pasadena, California 91103*

December 9, 1977

Refer to: 652-GAM:sc

NASA Scientific and Technical
Information Facility
P. O. Box 8757
Baltimore-Washington International Airport
Maryland 21240

Attention: NASA Representative (S-AK-RKT)

Gentlemen:

Attached are COSATI Technical Report Standard Title Pages for JPL Technical Documents released duirng October and November 1977.

Two copies each of the following JPL Publications are enclosed for your systems input and listing in the unlimited, unclassified, category of STAR:

*JPL Publication 77-36	Comparison of Experimental and Theoretical Reaction Rail Currents, Rail Voltages, and Airgap Fields for the Linear Induction Motor Research Vehicle.
JPL Publication 77-54	Evaluation of Coal Feed System Being Developed by ERDA.
JPL Publication 77-55	Proceedings of the Conference on Coal Feeding Systems. Held at the California Institute of Technology Pasadena, California, June 21-23, 1977.
JPL Publication 77-59	An Analysis of the back End of the Nuclear Fuel Cycle with Emphasis on High-Level Waste Management.
JPL Publication 77-60	High Efficiency Thin-Film GaAs Solar Cells.
JPL Publication 77-61	Monopropellant Thruster Exhaust Plume Contamination Measurements Final Report.
JPL Publication 77-65	Development of a Multiplexed Bypass Control System for Aerospace Batteries.
JPL Publication 77-66	Sampled Data Analysis of a Computer-Controlled Manipulator.
*JPL Publication 77-68	Investigation of Pressure Oscillations in Axi-Symmetric Cavity Flows. Final Report-Phase I.

JET PROPULSION LABORATORY *California Institute of Technology • 4800 Oak Grove Drive, Pasadena, California 91103*

NASA STIF

December 9, 1977

JPL Publication 77-71 Sharing the 620-790 MHz Band Allocated to Terrestrial Television with an Audio-Bandwidth Social Service Satellite System.

JPL Publication 77-72* Medical Ultrasonic Tomographic System.

* The Standard Title page is included with the Publication as a part of the customer format.

Copies of the following report for which a Standard Title Page is enclosed, were released to NASA for unrestricted systems input and announcement at the time of initial distribution:

DSN PR 42-41 Deep Space Network Progress Report

Two copies of the following JPL Civil System Project Office Documents required under the terms of their particular contracts are enclosed and authorized for your systems input and listing in the unlimited, unclassified category of STAR:

5040-3 Building Application of Solar Energy, Study No. 2: Representative Buildings For Solar Energy Performance Analysis and Market Penetration.

5040-10 Building Application of Solar Energy, Study No. 4: Utilization of Solar Energy in Southern California Buildings.

Very truly yours,

for Joseph A. Wynecoop, Manager
Information Support Section
Technical Information and
Documentation Division

Enclosures:

cc: Jerry Waldo, Acquisitions Branch

JPL PUBLICATION 77-72

Final Report: Medical Ultrasonic Tomographic System

Richard C. Heyser
Dennis H. Le Croissette
Robert Nathan
Jet Propulsion Laboratory

Robert L. Wilson
Harbor General Hospital, Los Angeles

October 1, 1977

Prepared for

National Institutes of Health
Division of General Medical Sciences

by

Jet Propulsion Laboratory
California Institute of Technology
Pasadena, California 91103

PREFACE

The work described in this report was performed by the Earth and Space Sciences Division of the Jet Propulsion Laboratory for the National Institutes of Health, Division of General Medical Sciences, under Grant No. GM23094-01.

ABSTRACT

An electro-mechanical scanning assembly has been designed and fabricated for the purpose of generating an ultrasound tomogram. A low cost modality has been demonstrated in which analog instrumentation methods form a tomogram on photographic film. Successful tomogram reconstructions have been obtained on in-vitro test objects by using the attenuation of the first path ultrasound signal as it passes through the test object. Thus, the nearly half-century tomographic methods of X-ray analysis have been verified as being useful for ultrasound imaging.

CONTENTS

FIGURES

FIGURES (Contd)

Summary

An electro-mechanical scanning assembly has been designed and fabricated for the purpose of generating an ultrasound tomogram. A low cost modality has been demonstrated in which analog instrumentation methods form a tomogram on photographic film. Successful tomogram reconstructions have been obtained on in-vitro test objects by using the attenuation of the first path ultrasound signal as it passes through the test object. Thus, the nearly half-century tomographic methods of X-ray analysis have been verified as being useful for ultrasound imaging.

Good geometric reconstruction of simple objects has been obtained over a field of 6 cm by 8 cm. With a system bandwidth of 1 MHz, centered at 2.5 MHz, and unfocussed transducers measuring 5 mm in diameter, a resolution of approximately 3 mm has been demonstrated by using the coherent signal processing technique known as time delay spectrometry. Computer simulation has yielded results sensibly in agreement with the analog experimental data. Thus, the original objectives of this grant have been successfully met.

Additional considerations have been revealed by the many physical measurements which were made during the course of the task. First, although quite acceptable images are obtained by using photographic film as the reconstruction medium, the inability of film to subtract light values creates an average background bias level on the tomogram. Discrete element memory matrices show promise of replacing film as a low cost reconstruction medium. Second, the need for an adaptive time window for accepting the earliest sound has been noted for those objects which are both highly elongated in geometry and exhibit substantial deviation of acoustic velocity from the surrounding medium.

Background of Tomogram Technology

It is a well known fact that it is possible to infer the structure of a multidimensional object from a set of its projections (see Appendices A and B). The mathematical basis for this reconstruction dates back to 1917 (1). The first practical use of this to medicine is due to Ziedses des Plantes (2), who formulated the basic principles of X-ray tomography.

His work pioneered what is now called body-section radiography, and his original techniques proved quite successful in clinical application. The des Plantes process produces images by preserving the differential attenutation profile of a planar cross section. The images are built up on a photographic emulsion. An X-ray point source and a film cassette are articulated about the object in such a manner that all points on the tomographic plane are constrained to remain invariant on the film, while points not on the tomographic plane are blurred by the scanning motion of film and X-ray source. As the scan progresses, the image of the tomographic plane is continuously reinforced, while the other subject planes are blurred by the scanning motion. As simple as this concept might be, even considering the limitations of the usable range of film exposure, the results were considered clinically useful for more than four decades.

What makes this technique work is the fact that X-rays principally react through differential absorption and seldom rebound to create significant diffraction of reverberation. Working against this technique is the weak interaction of X-radiation with soft body tissue and the additive properties of film which build up both the out of focus as well as the focussed parts of the image.

The advent of computerized axial tomography (CAT) has virtually eliminated these difficulties. Computer memory, rather than film, is the storage medium and signal values can thus be processed as desired. The weak interaction with soft tissue is not eliminated in CAT, since

this is a result of the physics of the process, but differential attenuation can be extracted for more efficient image formation.

Whereas, with des Plantes' original film method, the tomograph plane was essentially perpendicular to the line of centers between X-ray source and film, CAT creates a tomograph plane defined by the X-ray path. This change of plane has been regarded as an improvement in CAT since the image format includes the outer boundaries of the object being viewed.

There is one serious drawback with present CAT relative to des Plantes' original method, and that is its cost. The type of equipment required for scanning and the nature of computer reconstruction has elevated the cost of such equipment well beyond what a small clinic might afford. In addition, the use of X-rays still poses a hazard, no matter how slight, to the patient who is scanned. Finally, the physics of tissue/X-ray interaction still present a limitation to the subtleties of tissue pathology which can be visualized in the presence of photon noise.

Ultrasound, unlike X-ray photons, interacts strongly with soft tissue; and the interaction is of a nature quite different than that of photons. X-ray photons do not sensibly speed up or slow down in passage through tissue. But, ultrasound velocity is itself an indicator of one aspect of tissue property. The differential absorption of ultrasound is due to factors which are different than those which cause absorption of X-ray photons. Thus, it can be argued that even if X-ray CAT had no safety or cost problems, it is worthwhile to pursue ultrasound tomography since it visualizes other tissue properties. Ultrasound can thus complement X-ray images.

It was recognition of these factors which led to the work discussed in this report. It was decided to investigate the use of ultrasound for the generation of a tomogram. The format of this tomogram is to be of

the type now obtained with CAT. An ultrasound source and receiver are positioned on opposite sides of the object to be scanned. A method is used that selects the earliest sound through the object, which has the greatest likelihood of being the direct sound analogous to the X-ray path. This sound is processed to produce a signal proportional to the true energy of signal passage, regardless of waveshape deformation due to differential frequency attenuation of the intervening tissue. The reconstructed tomogram is then converted to a photographic image for observation and analysis.

It was the intent of this task to find out just how inexpensively it might be possible to generate an ultrasound tomogram, recognizing that to do so will produce a sub-optimal image. The question was, are the results of the lowest cost tomogram still clinically useful? Or, in colloquial language, if one removes all the bells and whistles, is it possible to envision a class of instrument that could find use in small clinics? The result of this present investigation is an affirmative answer to these questions.

References

(1) J. RADON, Ueber die Bestimmung von Funktionen durch ihre Integralwerte laengs gewisser Mannigfaltigkeiten (On the determination of functions from their integrals along certain manifolds), Berichte Saechsische Akad. Wissenschaft. (Leipzig), Math. Phys. Klass 69, pp. 262-271.

(2) Ziedses des Plantes, "Eine neue Methode zur Differenzierung in der Roentgenographie," Acta Radiol., vol. 13, 182-192, 1932.

Definition of Terms

X-Ray and Ultrasound Tomography

In medical terminology, the word tomograph traditionally referred to an X-ray photograph of a selected plane in the body. It had the geometrical appearance of a tissue cross-section. The advent of ultrasound imaging using pulse-echo techniques led to a format that was geometrically identical to the X-ray tomograph in the choice of coordinates, but was an image of ultrasound reflection properties and not those of electromagnetic radiation. By convention, this type of image came to be known as an ultrasound tomograph.

Up to the present time, this duplication of terminology could cause no confusion because of the different modalities involved. However, the recent introduction of image reconstruction methods capable of generating a sectional view from transilluminated projections may already be the source of some confusion, particularly in the case of ultrasound.

There are, at present, three basic types of tomograph images, one using X-rays and two using ultrasound. The information contained within these images is complementary. With very few exceptions the images will show different information. One is not a replacement for the other.

The differences among the three tomographs may be seen by inspecting the three images of the same section of the body. One of these will be an X-ray tomograph and will show the differential attenuation of tissue for X-rays passing through that tissue. The second will be a conventional ultrasound pulse-echo tomograph and will outline the boundaries between tissue of different acoustic impedance by indicating the amount of sound reflected back from those boundaries. The third will be an ultrasound tomograph made by reconstructing the information obtained by the passage

of ultrasound completely through the section. This portrays the differential attenuation for sound due to passage through various types of tissue.

With the exception of the external boundaries of the subject and a few dominant structural characteristics, these three types of tomograph probably will not look alike. That does not mean that any one is better than another. Rather, it means that the type of information contained within them is different. Each kind of tomograph can reveal a great deal of information to someone experienced in interpreting that particular type of image. What is potentially more significant, however, is the synergism that may occur with two or three types of tomograph, each revealing its own peculair set of information. This could lead to a diagnostic capability not available from the use of any single type of tomograph.

The class of tomograph which this report deals with is that obtained from a measure of the ultrasonic energy that passes completely through the tissue. This is an ultrasound transmission (or attenuation) tomograph and, in a general sense, is the acoustic analog of the X-ray tomograph. Because of the more complete control and processing that can take place with ultrasound signals, a great deal more relative information is obtained from this ultrasound signal than is obtained from X-rays alone.

Design of Analog Equipment

As proposed, an attachment was developed for converting the existing JPL rectilinear scanner to a tomograph scanner. The rectilinear scanner uses two precision stepper motor drives mounted at right angles. Transmitting and receiving ultrasound transducers are mounted on a rigid yoke assembly and articulated in a raster, scan fashion about a test specimen. The transducers are positioned so as to be on opposite sides of the test specimen and are mounted such that the major axis of the two transducers are aligned for transillumination of the specimen.

The scanner provides two degrees of translational motion, but does not provide rotational motion about the test object. Because of the substantial mass of the drive mechanism, it was not considered feasible to convert the drive to provide tomographic reconstruction. A simpler solution, and one consonant with the requirements of this task, was to rotate the specimen and allow the scanner to translate the ultrasound probes past it in such a manner that the ultrasound signal always remained in one plane through the specimen regardless of position. The manner in which this was done was outlined in Figure 5 of the proposal and is reproduced here as Figure 1 of this report.

A multiple-position rotary switch of robust construction was procured and used for support of the specimen as well as an angle pickoff. A 48-position indexing switch provides repeatable angle measurements every 7.5 degrees around the whole of the test object.

Electrical signals corresponding to the sine and cosine of the angle of test object rotation relative to scanner axis are obtained from two quadrature wipers on the switch assembly. Precision resistor ladders are tapped by the wipers to provide the equivalent of a discrete sine/cosine potentiometer.

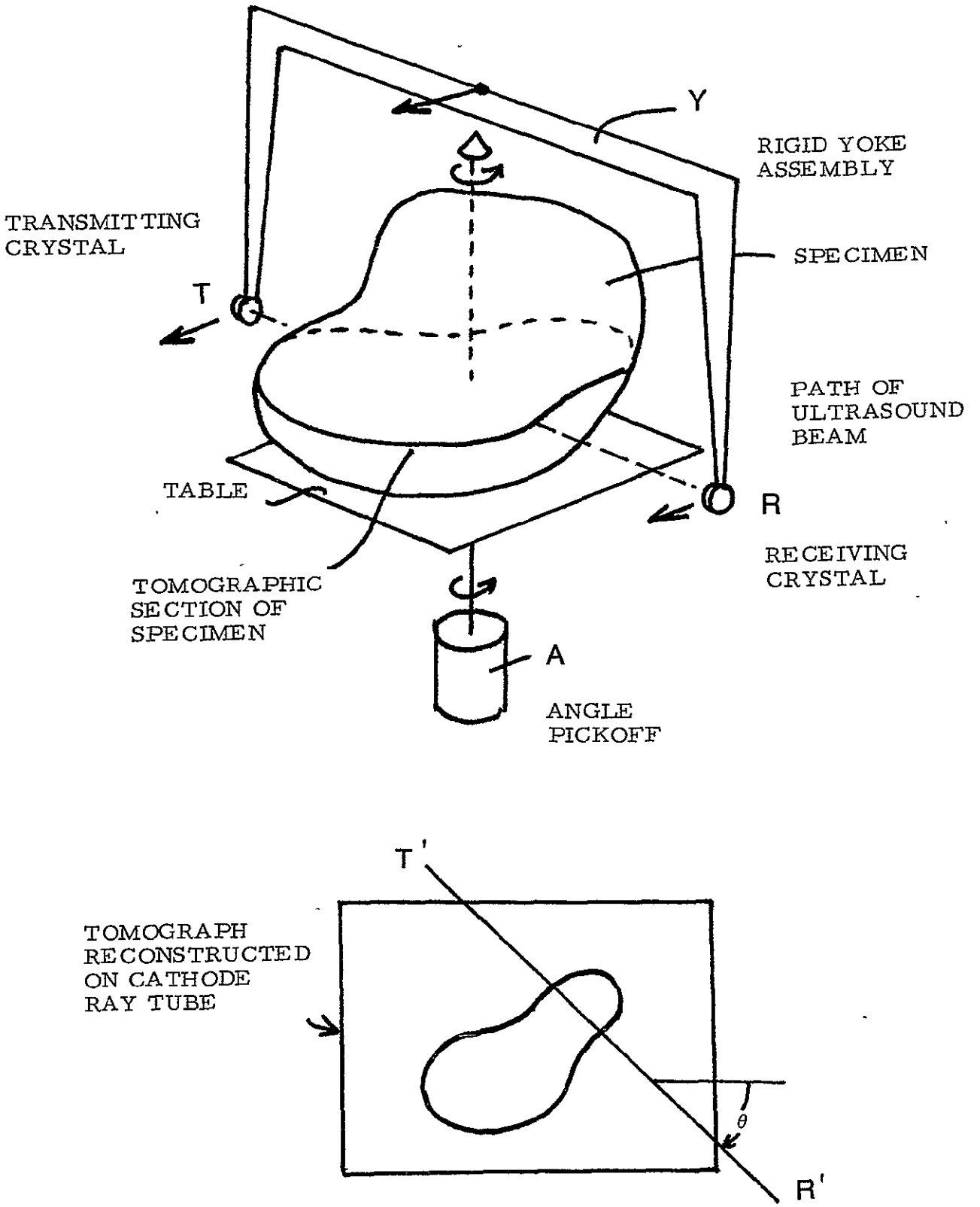

Fig. 1. Symbolic Representation of the Combined Physical Translation of Ultrasound Crystals and Rotation of Test Object Which is Used to Generate a Tomographic Image.

The purpose of the electrical pickoff is to allow a multiplicity of angular views to be taken and registered with respect to the probe scanning geometry. The angle pickoff is processed to provide a modified C-mode scan on a display tube. In the visual presentation, the coordinates of the display device are fixed to those of the object being scanned. As the object is rotated for subsequent views, the horizontal and vertical drive to the display tube is inversely programmed so that the reconstructed object remains firmly placed on the face of the tube. The reconstruction geometry is, thus, such that a fixed point on the tomographic section corresponds to a fixed point on the face of the display tube. Arithmetic reconstruction of the tomograph is performed by utilizing a photographic place to "add" the spot intensity at each place on the eventual tomograph. The basis for this is the time-exposure reciprocity known to exist over a limited range on all photographic emulsions.

A simplified diagram of the electronic circuitry designed for the display tube drive is shown in Figure 2. In order to simplify the diagram, only that circuitry necessary to provide the modified C-mode scan is shown. There was a moderate amount of additional circuitry required to interface with JPL's specialized equipment, but that is not essential to an understanding of the operation of the tomograph scanner.

The signal referred to in this figure as the horizontal input is a voltage proportional to the translational position of the scanner. Two additional voltages are added to this translational position signal. A one-kilohertz sawtooth of fixed amplitude is added for the purpose of creating a straight line on the face of the display tube. This straight line will create the trajectory of the geometric path of the ultrasound signal passing through the test object. The second signal added to the horizontal input is the tomographic center control. This allows the operator to readjust the center of the cathode ray display to be aligned with the center of the test object.

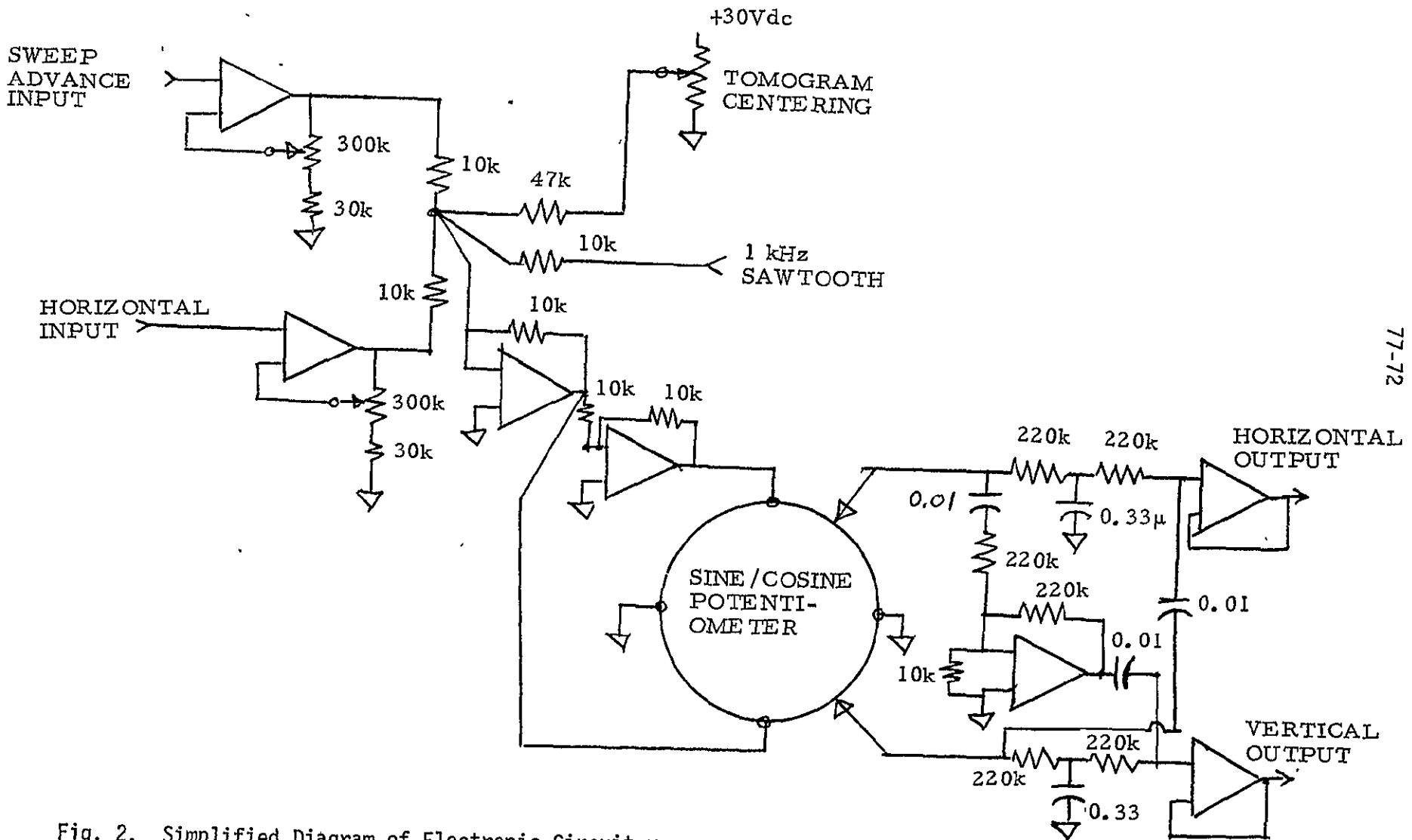

Fig. 2. Simplified Diagram of Electronic Circuitry

These three signals are sent in anti-phase relationship to the multiple-position rotary switch. In this diagram the 48-position switch is symbolized by the circle, denoting the series-connected resistors that connect adjacent terminals. There are two wiper arms mounted at ninety degrees with respect to each other. These are symbolized by the arrows.

In order to provide a straight line on the screen which is in quadrature with the direction of mechanical scan, and thus aligned with the ultrasound energy, it is necessary to provide the low-pass and high-pass circuitry that follows the rotary switch pickoff. This circuitry directs the low-frequency voltages of translational motion to one axis and the high-frequency sawtooth voltage to the quadrature axis of the display tube.

Test Results

The general results of the experimental program are perhaps best presented as resultant photographic images. Throughout this program it was decided to use Polaroid film of the type commonly used to photograph ultrasound images. It was realized that such film, with its very high contrast, is a poor choice for use in reconstructing tomographic images. Nevertheless, if the concept worked with such film, it would demonstrate an extremely low cost modality.

In all cases, an open shutter exposure mode was used and the final image obtained as a superposition of all scans. The cathode ray display was carefully adjusted so that the major reticle marks which are seen in these images corresponded to one centimeter calibrations in the object space. The test objects were carefully positioned to lie in various random positions relative to the geometric center of the tomogram reconstruction. This was done in order to assure that no inadvertent image improvement could occur if, for some reason, the geometric reconstruction depended upon the relative position of the object and scanner.

Both 360 degree reconstructions and 180 degree reconstructions were made on a number of test objects. No difference could be noticed between these views, which indicates the reciprocity of scan direction.

One of the first sets of test objects which were run is shown in Figures 3 and 4. This consists of a cross section of a circular hypodermic case and a 4-40 metal screw. The hypodermic case is one centimeter in diameter and approximately 1.5 millimeters in thickness. Except at grazing incidence, ultrasound passes through the lumen of the case. The metal screw is approximately 2 millimeters in thickness and represents a point scatterer smaller than the anticipated resolution of this system. Transmit and receive probes are 5 millimeter diameter, unfocussed discs and are 22 centimeters apart. The frequency range is 2 to 3 megahertz.

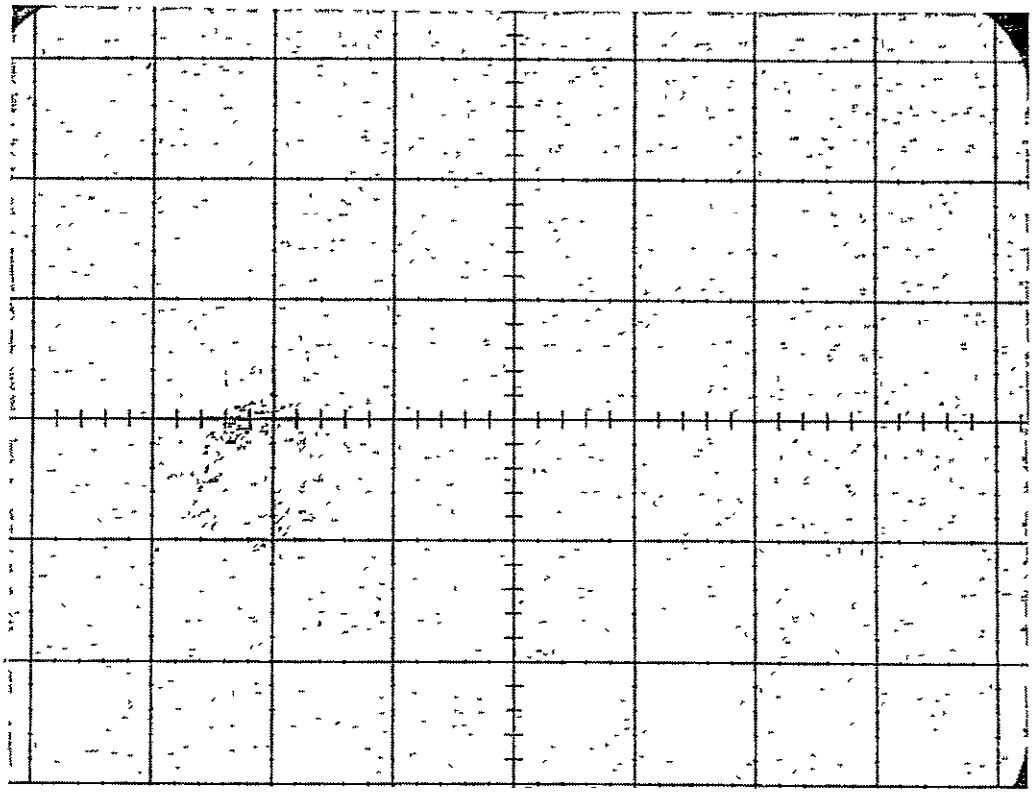

Figure 3. Positive Image of Hypodermic Case

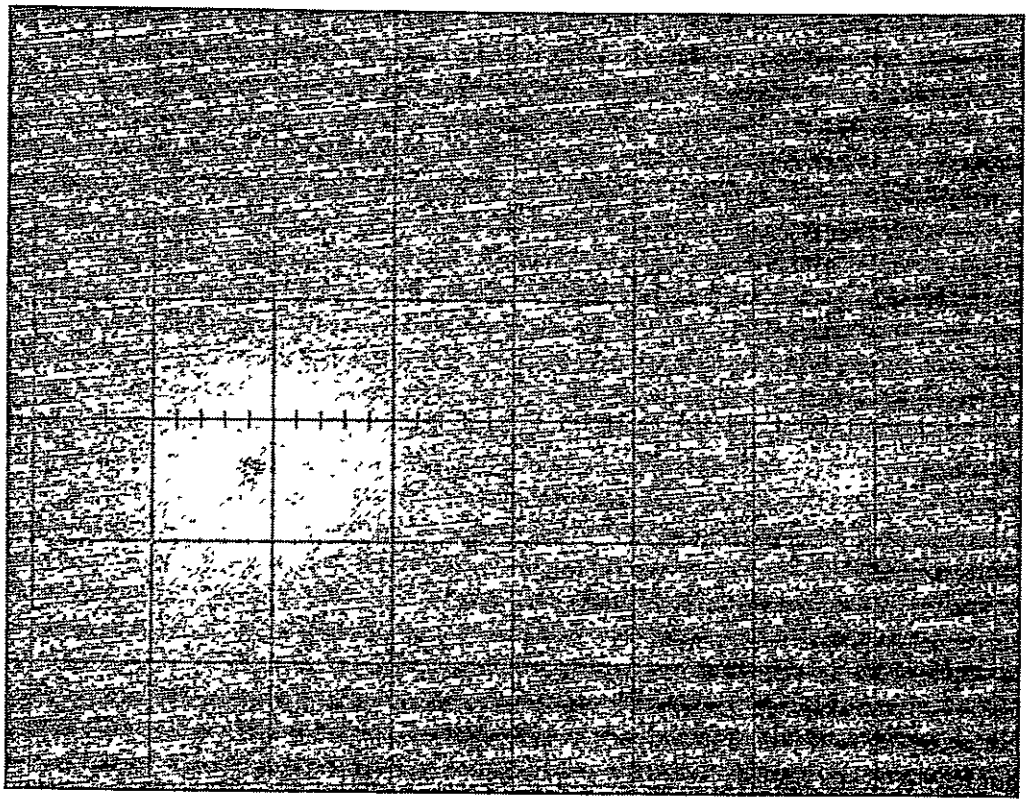

Figure 4. Rescan Image of Hypodermic Case Using Inverted Polarity

Figure 3 is a positive image and Figure 4 is a rescan using inverted polarity to the cathode ray intensity modulation. As anticipated, a point scatterer appears as a first-order Fresnel ring with about a 6 millimeter diameter. In Figure 3 the additive background is the result of using film which can only add, never subtract, light values. The geometric placement and configuration of the reconstructed image corresponds within a millimeter of the known position of these test objects.

Figures 5 and 6 are images of the hypodermic case alone. In Figure 6 the video signal to the intensity modulation terminal was high-pass filtered to determine whether edges could be sharpened by such simple means. The results are poor.

Figures 7 and 8 are two views of a low-contrast and high-contrast image, respectively, of a large diameter (1.3 cm) artery with associated soft tissue. This specimen is formalin fixed. The tomogram section is taken at right angles to the artery axis, just as the previous geometry of the hypodermic case, and the circularity of this section is in evidence. The shadowy outline around the periphery of the specimen is the outline of the plastic bag which held this sample in the water bath for tomogram scanning.

Figures 9, 10, 11, and 12 are images obtained on a kidney specimen which was formalin fixed and contained in a plastic bag. Figure 9 is a high-contrast transmission shadowgraph image obtained by the JPL raster scanning method. This image is the ultrasound analog of an X-ray shadowgraph and the method of obtaining such an image has been explained elsewhere. Figure 10 is a tomograph reconstruction of the density distribution in the plane lying 2.5 centimeters upward from the bottom of Figure 9. The small variation of sound energy through such kidney specimens causes an extremely low contrast in the reconstructed image. Nevertheless, a recognizable tomogram results. Figures 11 and 12 are tomograms corresponding to different levels through this object. The purpose in showing these results is to illustrate that in-vitro tomograms of tissue with small density variations do appear possible.

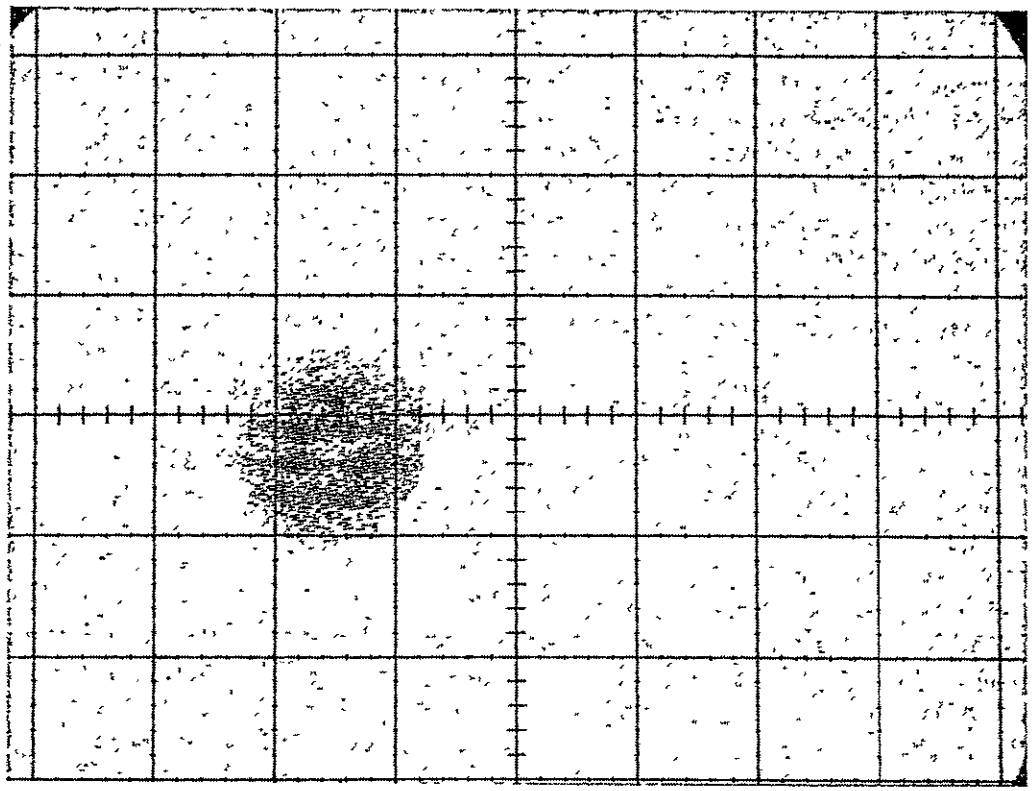

Figure 5. Reconstructed Image of Test Object

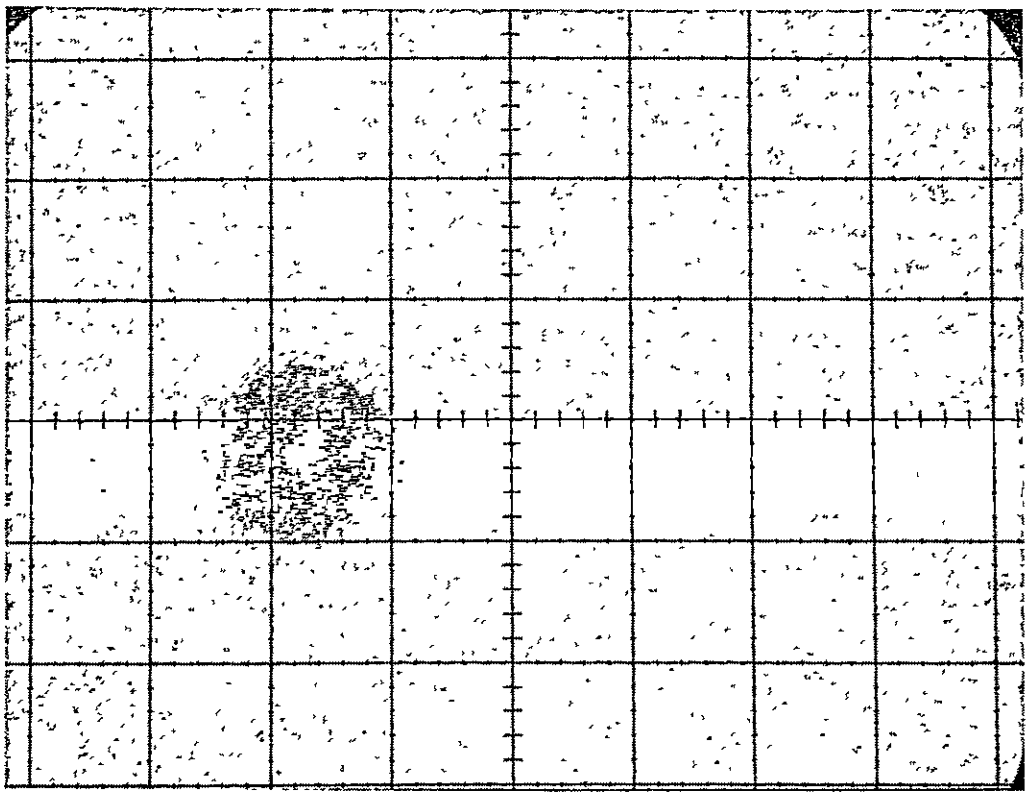

Figure 6. High-Pass Filtered Reconstructed Image of Test Object

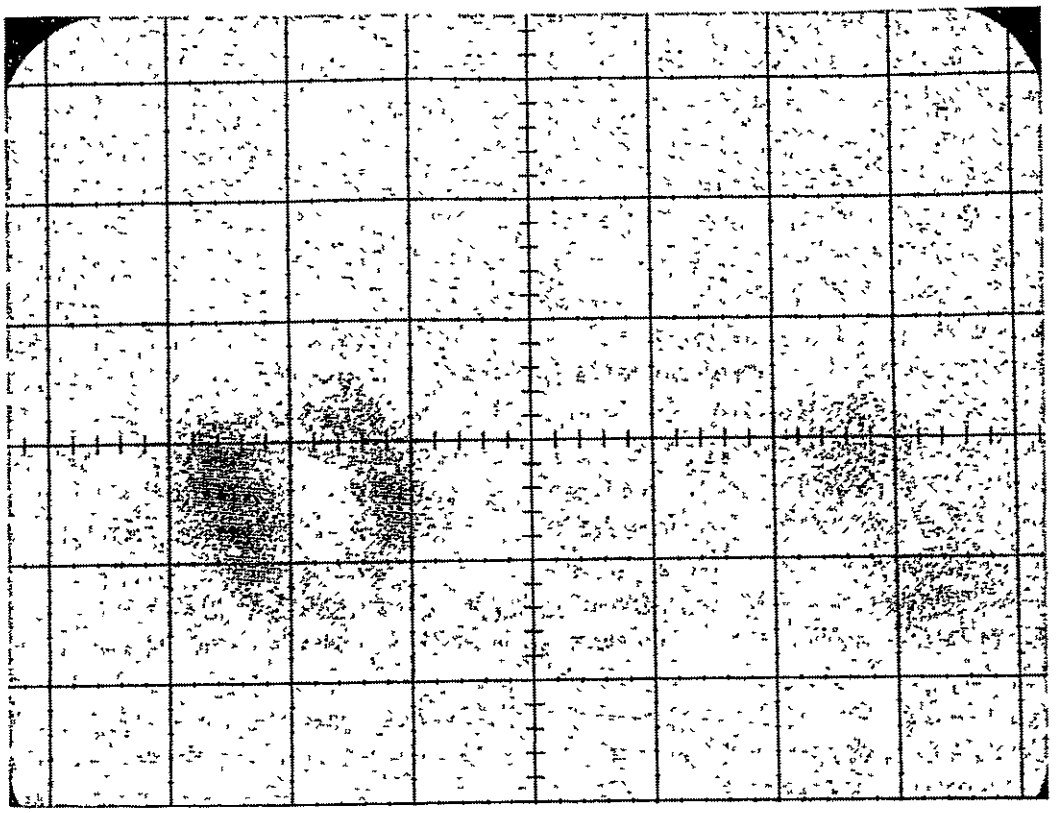

Figure 7. Low-Contrast Image of a Large Artery

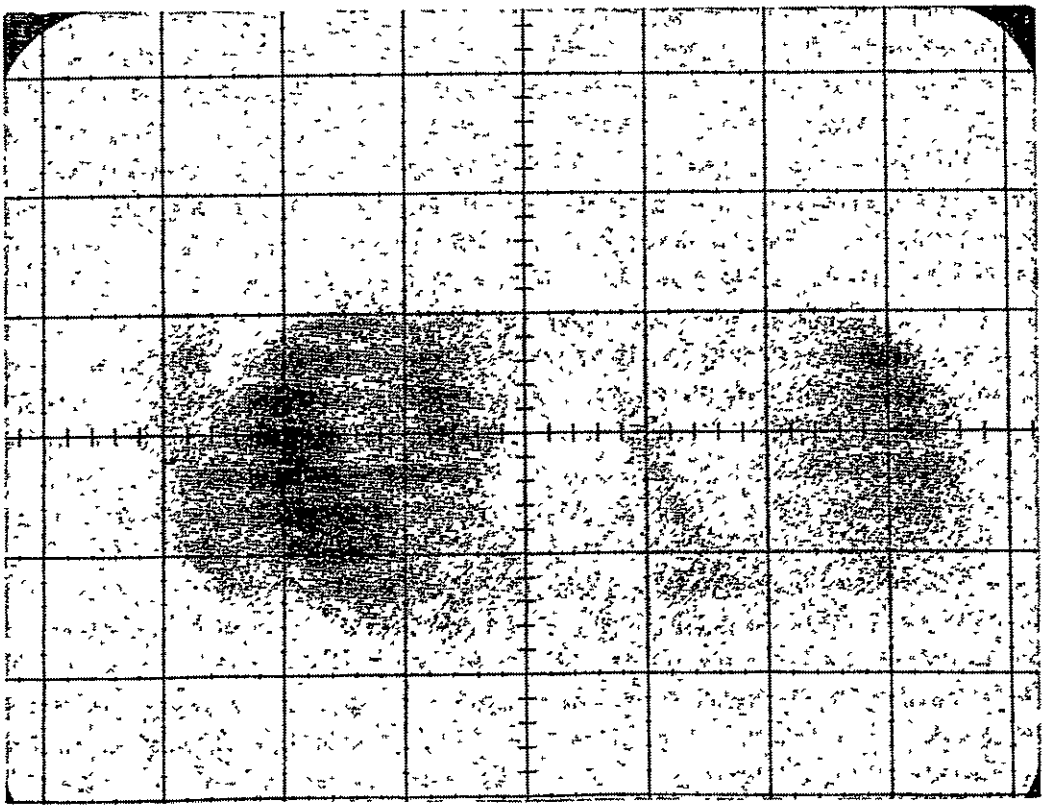

Figure 8. High-Contrast Image of a Large Artery

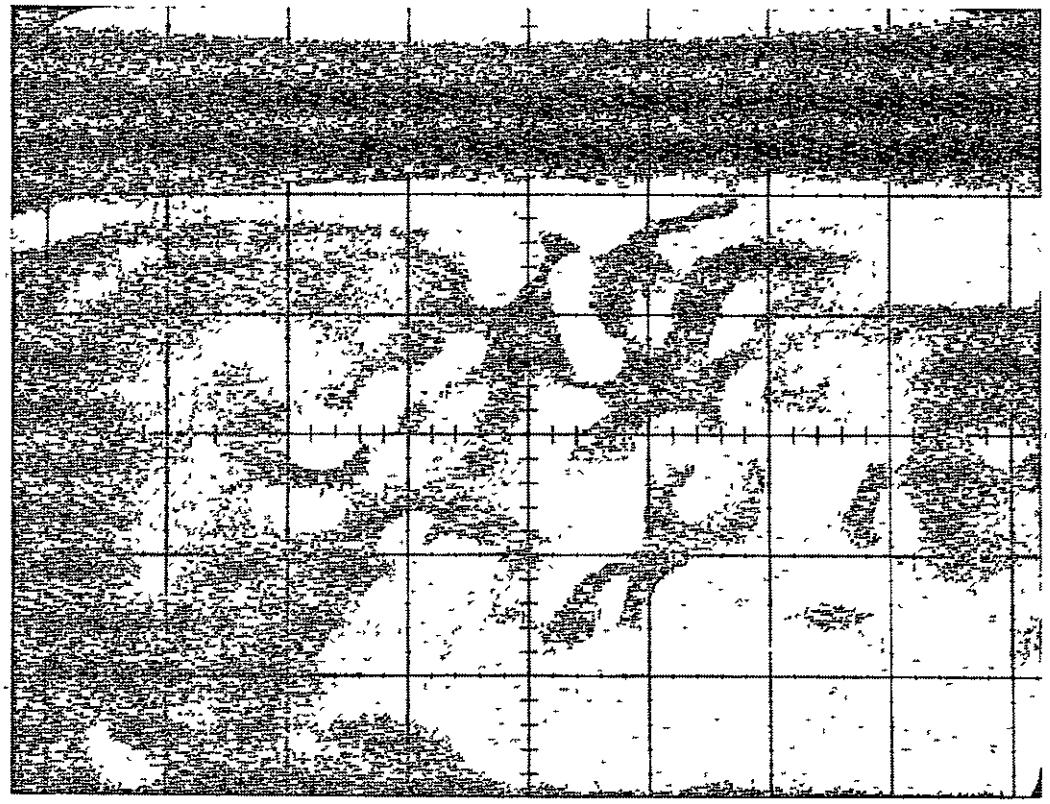

Figure 9. High-Contrast Shadowgraph Image by Raster Scanning Method of a Kidney Specimen

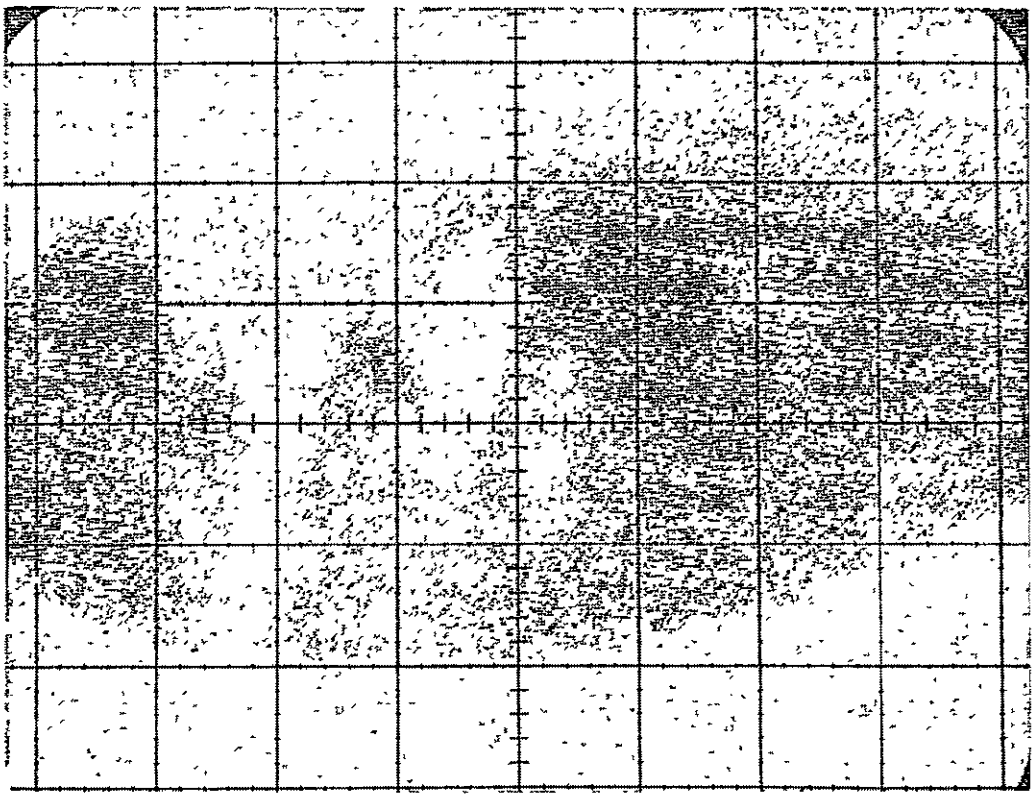

Figure 10. Tomograph Reconstruction of the Density Distribution of a Kidney Section

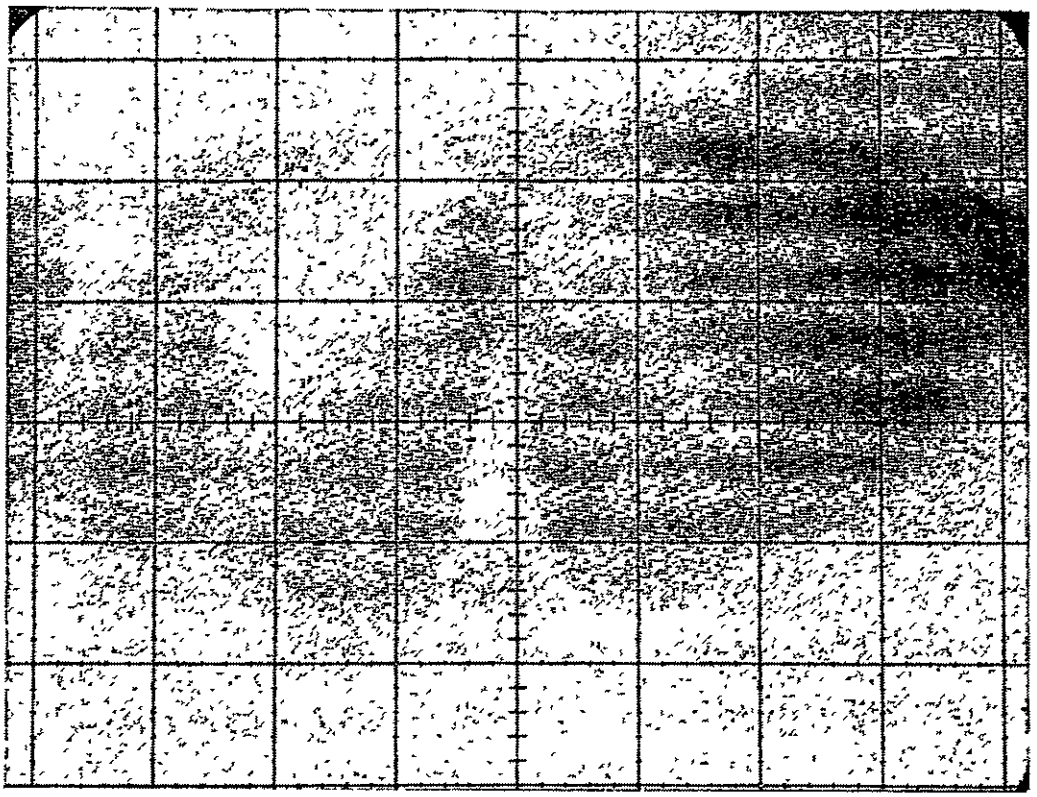

Figure 11. Tomogram at a Different Level of the Kidney Specimen

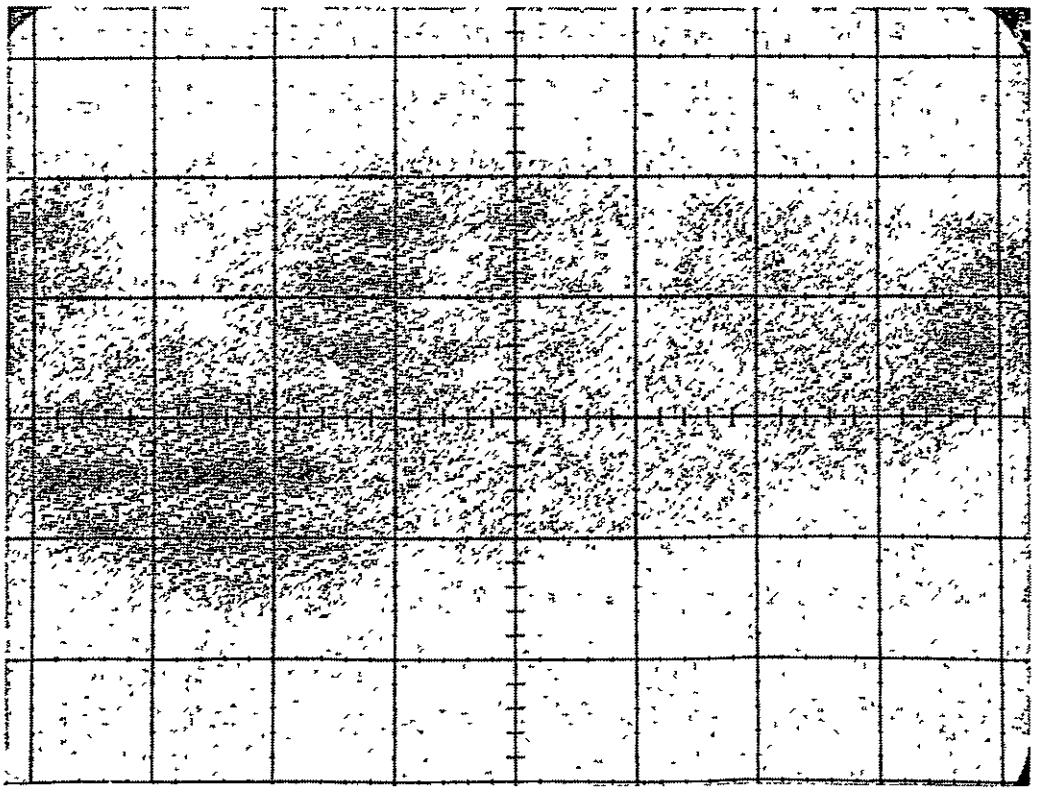

Figure 12. Tomogram at a Still Different Level of the Kidney Specimen

A more substantial variation in density produces stronger images, as shown in Figure 13. This specimen is one which has been used by this experimenter in a much earlier paper. It is a one-centimeter thick brain section containing two glioblastoma, which are distinguished under ultrasound analysis by an unusually high attenuation. The shadowy outline of Figure 13 is due to the bag containing the specimen. The small differential attenuation within the bag relative to the medium outside the bag is believed to be due to the interface attenuation between the bag and formalin. The edge of the brain section does not show in the tomogram reconstruction, possibly because of the masking effect of the shallow grazing angle, which the edge of the bag makes with those ultrasound rays parallel to the edge of the brain. However, the glioblastomas are well outlined and appear as the darker objects in the lower right quadrant of the image.

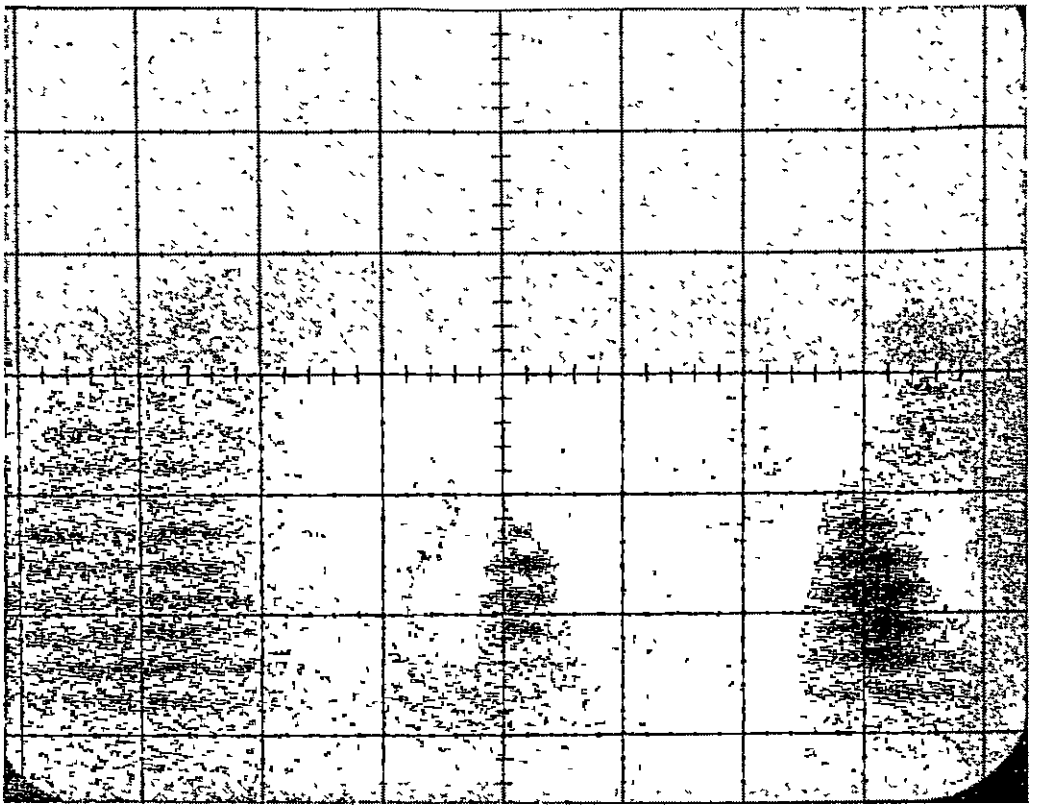

Figure 13. A Substantial Variation in Density of a Brain Section

Computer Simulation

Simulations were perfo.med in the Medical Image Analysis Facility at JPL. Most computations were made using a PDP-11/55 Computer System. The simulated images were created on a digitized image field of 100 samples by 100 lines. The distance between picture elements is set at 1mm of real space. For computational purposes, gray level intensities were quantified to 256 discrete levels (8 bits) although the display used in this task shows only 16 discrete levels.

Initial tests were performed on a single point of about 2mm diameter. (see Fig. 14A) Line integrals or projections were made at increments of 7-1/2°. Since the test object was rotationally symmetric, each projection should have been identical, but because of the coarse digitization, there were noticeable differences which were considered acceptable with regard to the assumed resolution limit of 2mm. In order to calculate an enhancement function later in this process, these projections were averaged together to give the following (projection A):

Projection A

Figure 14. Computer Simulated Tests on a Single Point: (a) Simulated Point Object, (b) Reconstructed and (c) Enhanced

Without using enhancement, each of the projected lines were then used as the source for the reconstructed image in back projection to give the image shown in Figure 14b.

There are some asymmetric characteristics in this reconstruction which are artifacts caused by digital roundoff. They can be corrected but the increase in numerical manipulation did not appear warranted.

This image was reprojected and the projections were again averaged to give the following (Projection B):

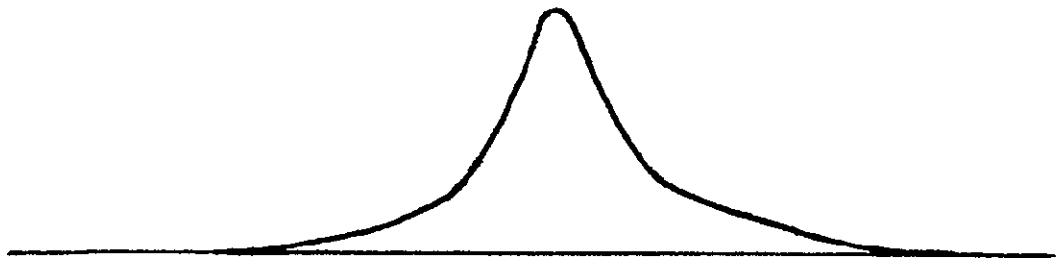

Projection B

The Fourier transform Projections A and B were calculated. The ratio of the amplitudes of the transforms (at each frequency) was made and the resulting ratio was used as input (with zero phase) for an inverse Fourier transform back to real space. The results were surprisingly brief (Projection C):

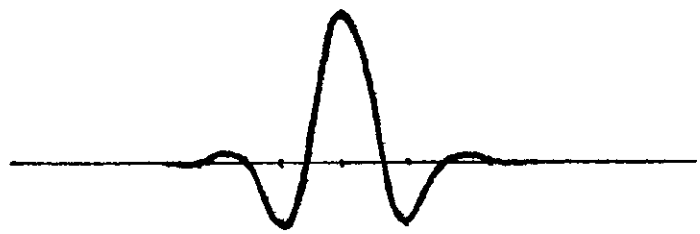

Projection C

This curve can be used as the enhancement kernel for convolution with each projection line prior to reprojection to compensate for the approximate $|r|^{-1}$ weighting which is implicit in the original reconstruction. Figure 14c shows the effect of applying this correction to the projections used to create Figure 14b. As was expected, along with the sharpened central peak, the sparse sampling in the number of projections has caused the spikes to appear more prominently.

A more complex test object was created with points simulating 1 and 2mm separations. (See Figure 15a) Its normal reconstruction and enhanced reconstruction are shown in Figures 15b and c respectively. Normal reconstruction does not appear to show either 1 or 2mm resolution whereas the enhanced image does distinguish the 2mm separations although the noise streaks are also prominent.

The syringe used in Figures 3 and 4 was simulated with three spheres at 2,3, and 4mm distance (see Figure 16). The computer program which generated the image, its projections, enhancement and reprojection is listed in Appendix C. Reconstruction was first performed using only 90° rotation sampling (at 7-1/2° intervals instead of the complete 180° sampling). A severe loss in resolution is evident (Figure 17a) and persists even if enhancement is performed (Figure 17b) although there is some recovery of detail.

Reconstruction using the complete 180° rotation is shown in Figure 18a.

A photometric analysis of the image density recorded on Polaroid film in Figures 3 to 13 was made with the following results:

Figure 15. Computer Simulation Tests on Separate Points: (a) Test Pattern with 1 and 2 mm Separations (b) Reconstructed, and (c) Enhanced

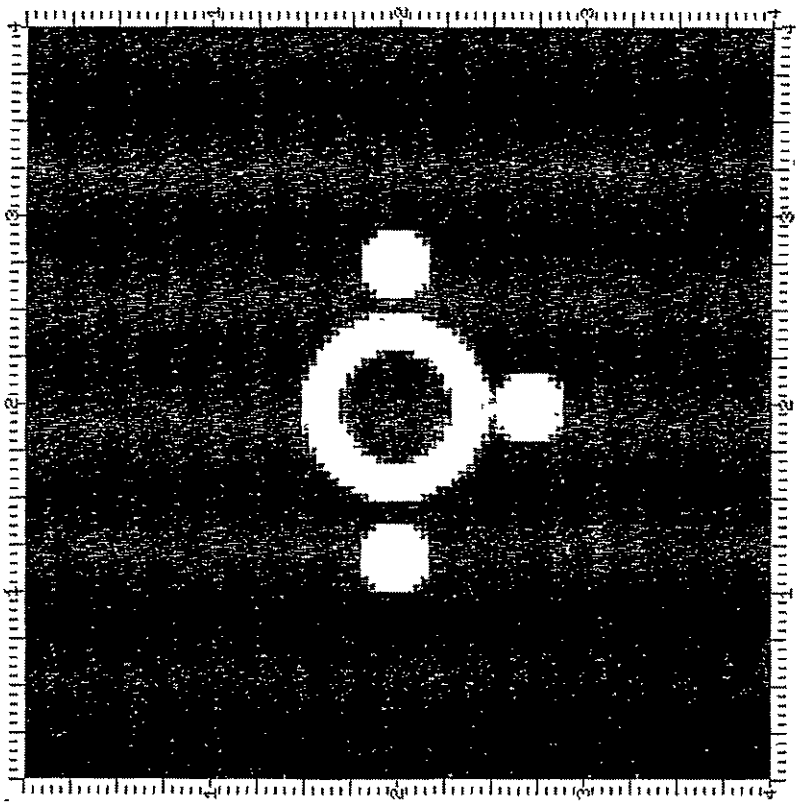

Figure 16. Computer Simulation of Syringe (as shown in Figures 3 and 4) Prior to Scan and Reconstruction

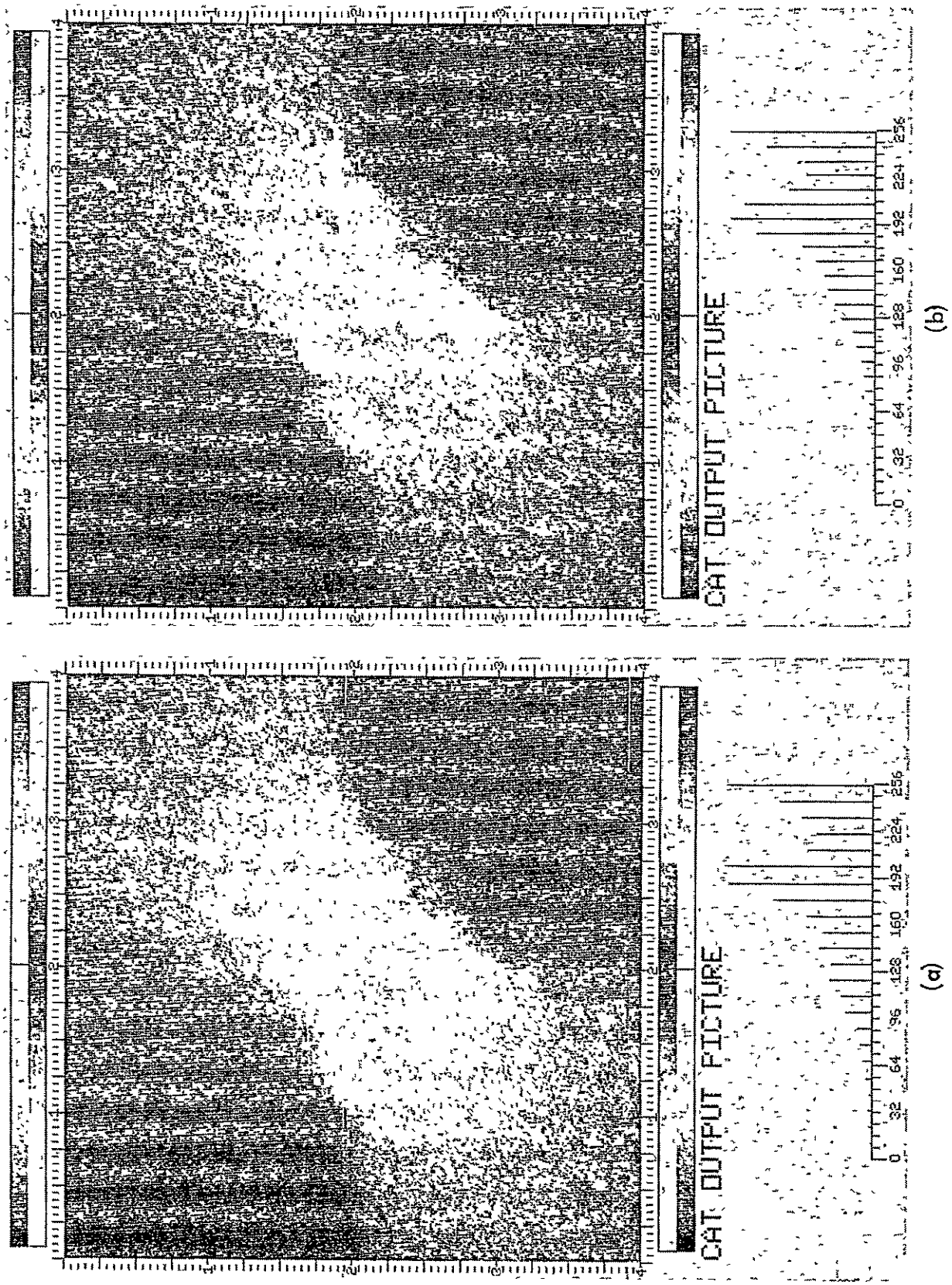

Figure 17. 90° Rotational Scan Reconstruction of Syringe (a) Normal Reconstruction, (b) Enhanced

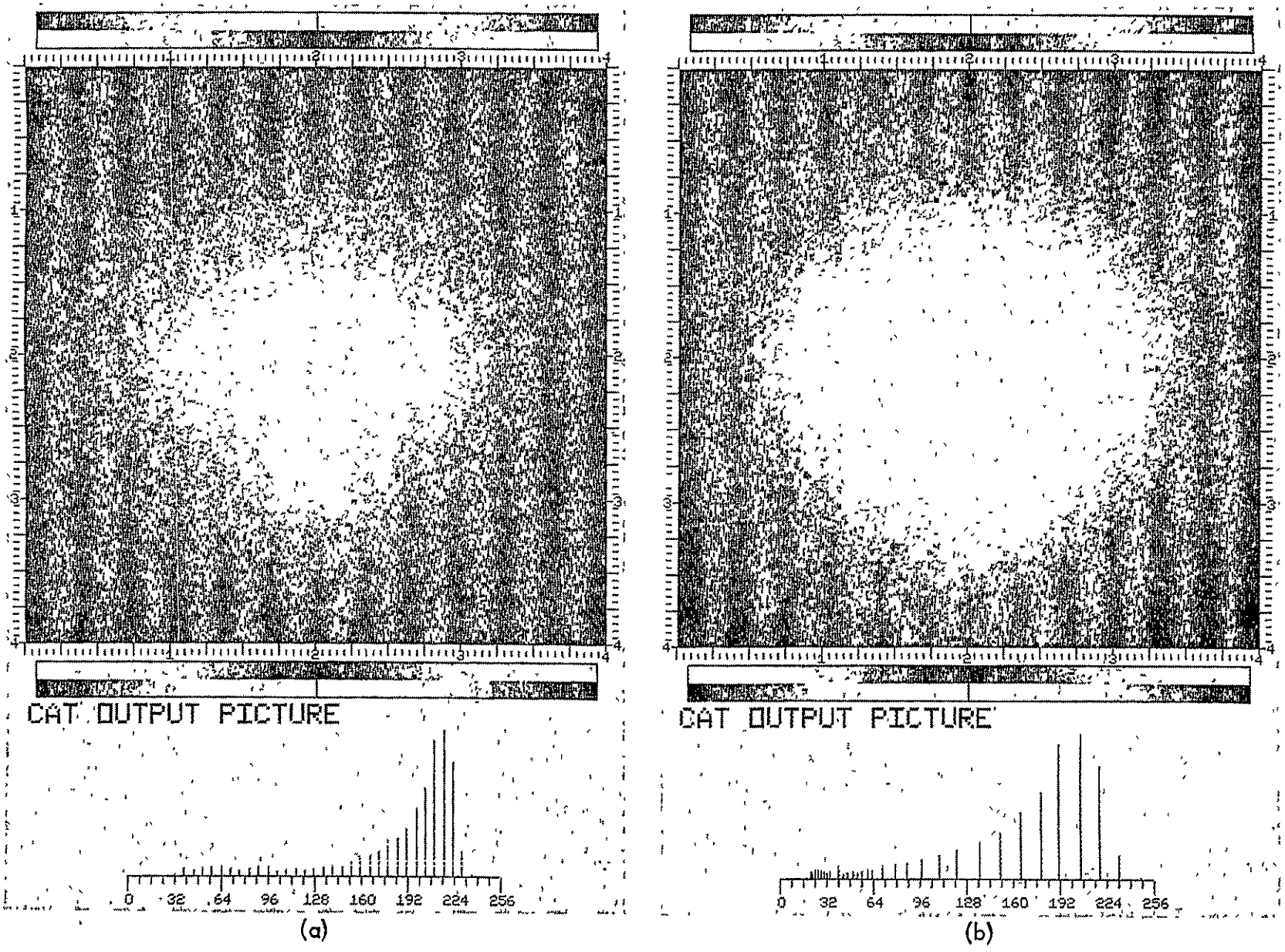

Figure 18. Full 180° Reconstruction of Syringe (a) Normal (b) Same as (a) but Photometrically Similar to Polaroid Film. (See Figure 4)

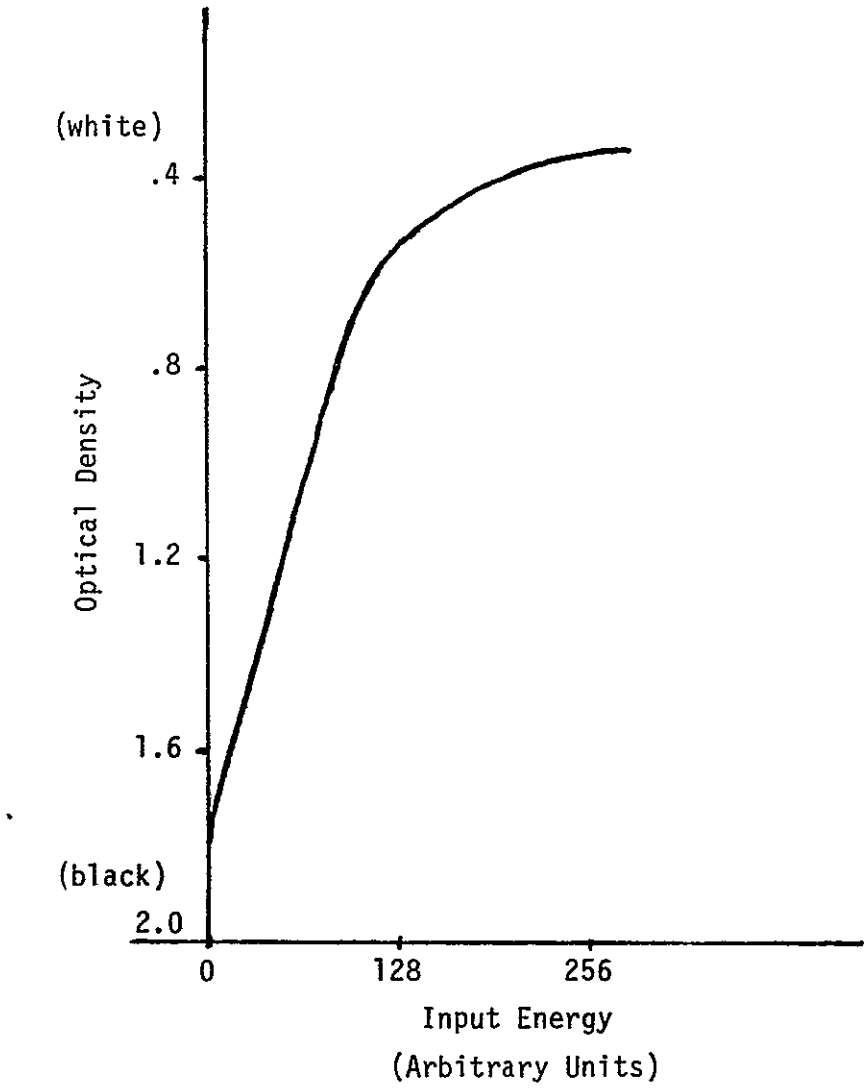

As the film receives more light, (as is used in one mode to represent less transmitted sound energy or a denser object), the image becomes less responsive to increases in exposure. The result is, that for objects which absorb (or reflect) sound energy, there will be a decreased sensitivity. As less of the input beam is seen by the sensor, then the film tends to saturate. Therefore, small differences in a dense object are washed out while background striations are visible (See Figures 18b and 4).

Enhancement sharpens this test object somewhat (see Figure 19a) and simulation of the film characteristics is shown for this enhanced image in Figure 19b. Again, the background is enhanced to the detriment of the detailed structure of the object of interest.

The polarity of the camera can be reversed, i.e., increased sound density provides increased film exposure (black). Figure 20a is the polarity reverse of Figure 18a. Figure 20b now shows a flat background and the three spheres are reasonably distinct.

Figure 21a is the polarity reverse of Figure 19b while Figure 21b is enhanced. Although the image is somewhat noiser, the objects are delineated more sharply.

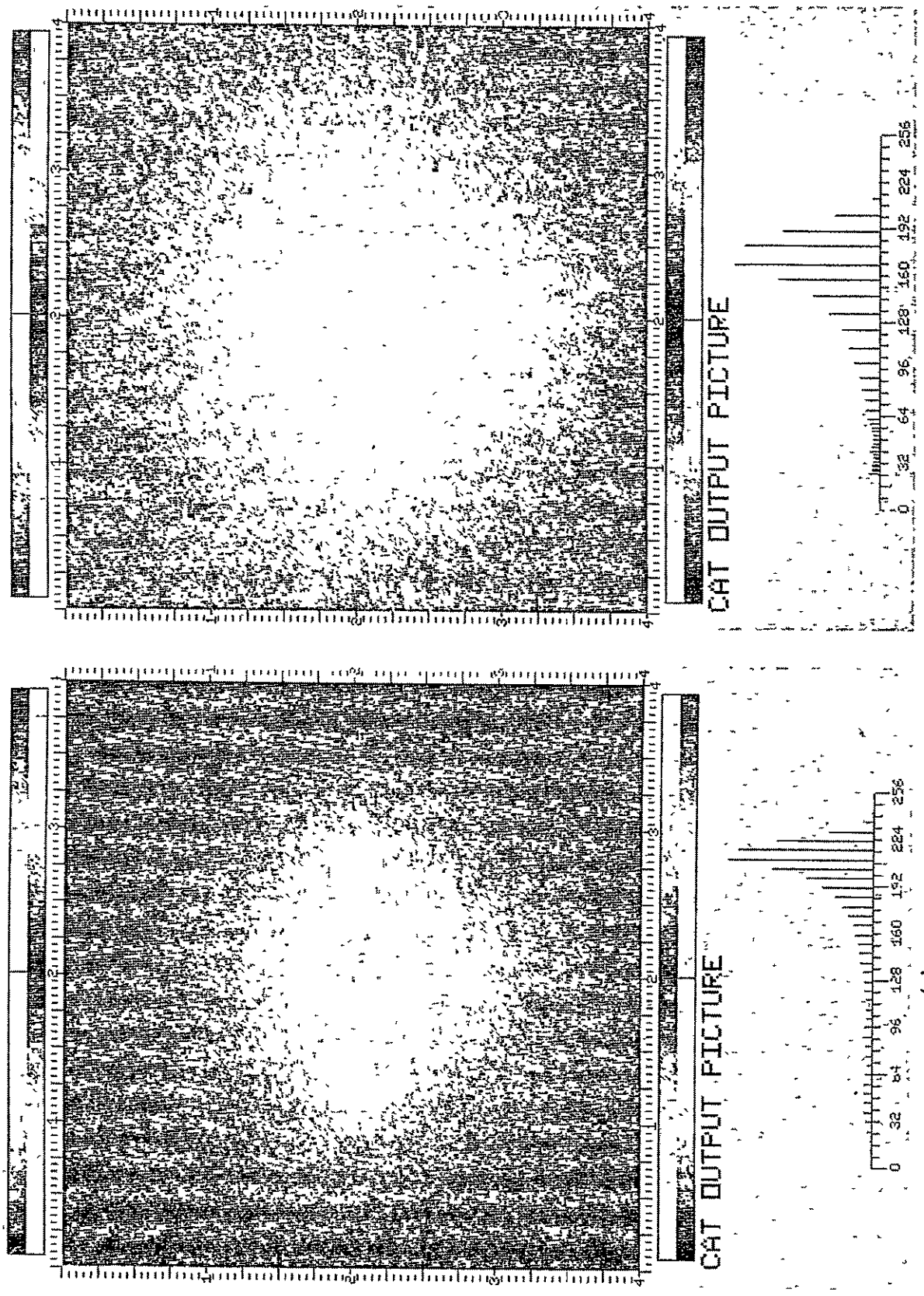

Figure 19. Same as Figure 18 But Enhanced (a) Normal Reconstruction (b) Polaroid Simulation

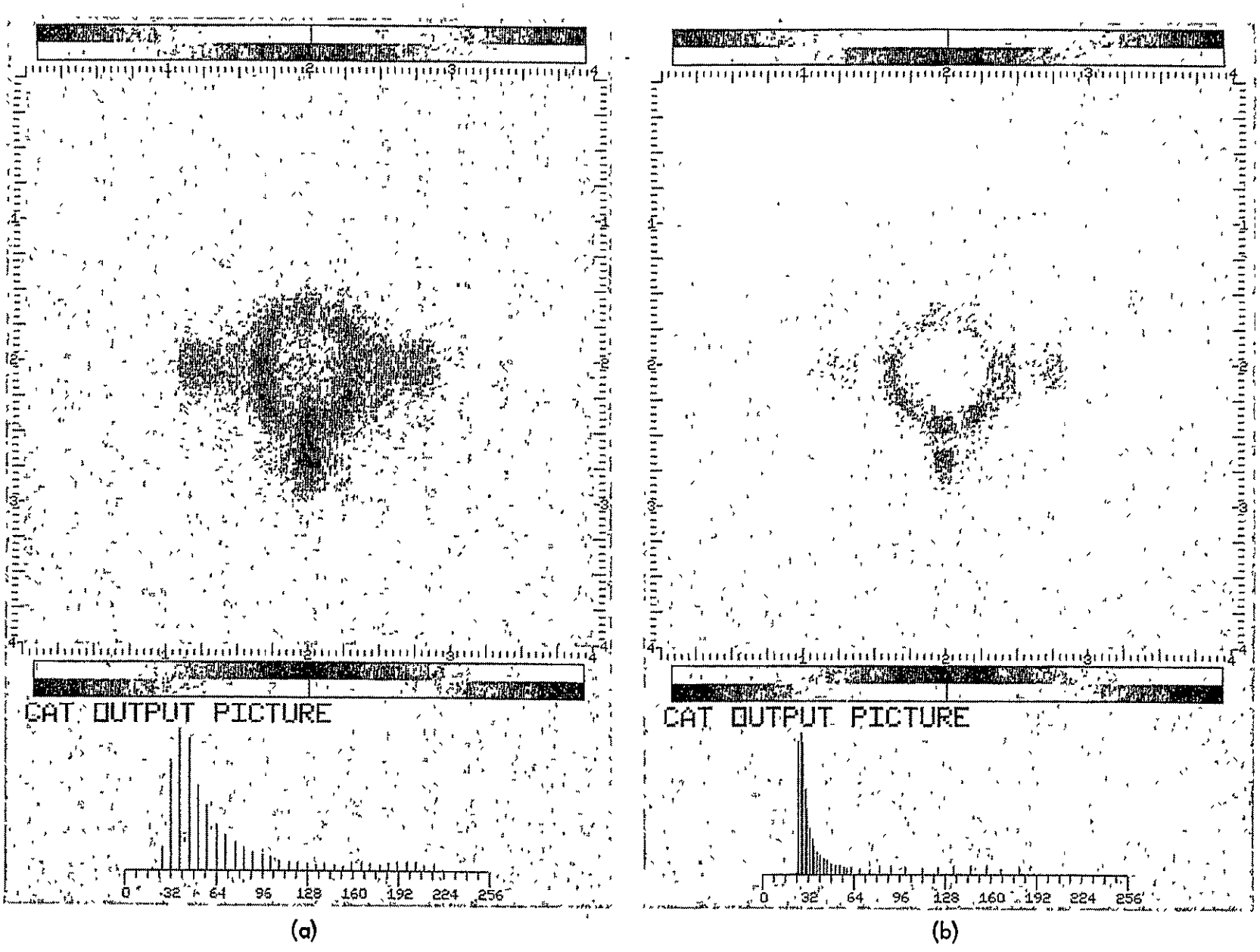

Figure 20. Reversed Polarity of Figure 18 (a) Normal Reconstruction (b) Polaroid Simulation

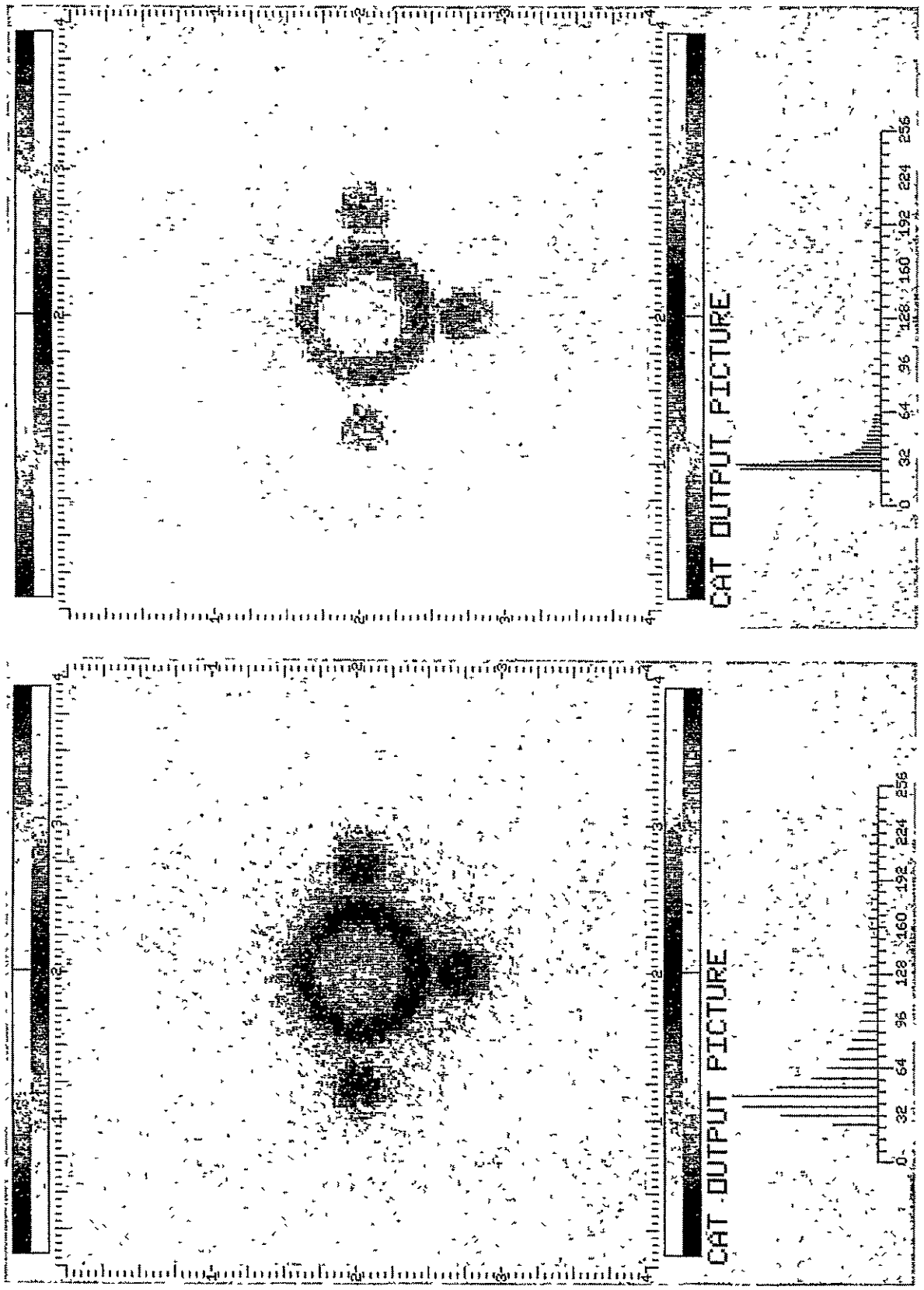

Figure 21. Reversed Polarity of Figure 19 (a) Enhanced Reconstruction (b) Polaroid Simulation

Discussion of Computer Results

The computer has been used to vary parameters and perform linear (additive as well as subtractive) and nonlinear operations and summations which are difficult to obtain through analog manipulation.

A major parameter is the redundancy of the recorded signal which occurs in overlapping scan regions. Also implicit are the gaps in information created by the large angular (7-1/2°) increments in the scanning sequences. In theory, with an infinitesimal angular increment, the redundancy factor approaches $|r|^{-1}$. In order to correct this error it is possible to enhance detail by convolving the reciprocal $|r|$ with the resultant final image. For the sake of removing noise it turns out that leaving the unenhanced image alone may appear more aesthetic and less distracting, but clinically important high frequency detail may be buried and lost in such a display. When the enhancement convolution is performed to recover fine details, not only is random high frequency noise made more visible but the error created by undersampling in angle is also made visible as "spokes" seen emerging from sharp points.

Enhancement can be performed very rapidly one-dimensionally by convolution of each projection with a one-dimensional projection of the $|r|$ convolution operator. For this work rather than use the theoretical factor of $|r|$, an experimentally evaluated enhancement factor was derived. Surprisingly, this function was determined to be a brief series of only three values -1.2, 3.4, -1.2 as seen in Projection C (p. 23). This function, when convolved with each scanned projection integral, provides the enhancement required to eliminate the redundancy of the low frequencies.

The results are as expected. It is not clear that 1 mm separations are distinguishable while separations of at least 2 mm are quite clear. (See Fig. 15C - p. 25)

Simulation of the nonlinear photometric response of Polaroid film also behaved predictably. Image detail whose brightness falls in the "toe" or saturated region of the film is lost. Digital memory as used in CAT or as simulated here provides greater dynamic ranges.

Finally, the ease of simulation illustrated in this effort and the recent availability of inexpensive digital microcomputers brings us to consideration of the next step - that of performing this entire operation with a real time microprocessor.

Additional Considerations

Time Delay Variations

In geometric terminology, the path or paths which ultrasound makes in passing through an inhomogenous medium are geodesic lines. It can usually be inferred that if there exists a curve of shortest traverse between two points in a medium, then it is geodesic. Geodesics can also be curves of greatest traverse, but in tomogram reconstruction we are interested in the minimum solution to the variational problem of energy passage.

Straight lines are geodesics for ultrasound only when there is no density change capable of bending the sound ray. If one reassembles a tomogram from integral projections and assumes the geodesics are straight lines when they are not, then the reconstructed image will be geometrically distorted.

JPL has had considerable experience in the reconstruction of transmission images using the integral projection as a measure of tissue interaction with transilluminating ultrasound. Successful transmission images have been obtained on in-vitro as well as in-vivo subject matter. This experience has shown that if the ultrasound energy corresponding to the shortest time of passage is used, and if subsequent signals corresponding to later, less direct paths are removed from the data, then reliable images result.

Consequently, the same type of signal processing was used in this tomogram task. The total signal energy density which arrives at the receiving transducer is processed and only those components taking a minimum time delay in passage, with a time acceptance of one microsecond, were used for image reconstruction. In order to use existing software, it was necessary to preset the time delay to one particular value for all angle positions of the test object relative to the transmitting and receiving of ultrasound probes.

For transillumination through one direction only, for example, imaging through the arm, this preset time delay and window of acceptance proves quite useful. It was for that purpose that our existing software was designed. However, when reconstructing multiple views taken at all possible angles for sound passing through highly elongated objects, this existing software is inadequate.

As an example: If within an irregular mass there are regions of differing acoustic velocity, the time delay of the earliest sound will vary about any previously preset time delay. If there is an elongated region of differing velocity within the mass, then the sound passing through the longest axis of that region may arrive at a substantially different time than the sound passing through the shortest axis of that region. That is what we observed when testing several in-vitro samples in which there was a path length variation of greater than 10 centimeters over the various angle projections and a tissue velocity considerably different than that of the fluid medium in which the specimen was placed. In such cases it is impossible to use a fixed-time delay for isolating direct from less direct ultrasound, and the tomographic reconstruction was not considered useful.

Refraction of sound did not pose the problem. The problem was due to extreme variations in arrival time, such that the energy came in and out of the one-microsecond time window. The solution to this difficulty was the use of an adaptive time delay which selects the earliest arriving sound energy and provides a time window around that early sound. If a pulse ultrasound system is used for this method of tomography, the simplest circuitry that one can use would be a threshold detector that enables a monostable timing circuit for opening and closing the time gate.

This software modification to optimize display by JPL's specialized instrumentation was not attempted during the course of this task since to do so would, in the experimenter's judgement, depart from the stated objective and divert funds from the goals that had been established. It has been adequately demonstrated during the course of this task that

detecting the first ultrasound signal and gating out subsequent signals provides sufficient data to reconstruct a usable tomogram. This methodology can be applied to existing pulse systems as well as the more powerful phase coherent systems.

Reconstructing Medium

Both the analog experiments and computer simulation, to be shortly described, have demonstrated that a simple arithmetic process produces usable tomograms. The principal difficulties with photographic film as a reconstruction medium are the lack of subtractive capabilities of photographic emulsion and the inherent nonlinearity of the exposure/density curve.

The nonlinearlity of exposure/density can be overcome by proper gain settings for adjustment of contrast. But film can only add light values, never subtract them. The result of this is the generation of a background bias level on the film which, in order to lie well above the knee of the exposure/density curve, must reduce the usable image contrast. This is a problem encountered in X-ray tomography which uses a film medium.

What is needed is a matrix array which can represent picture elements of the reconstructed tomograph and on which the values can be subtracted as well as added. When this present task was first contemplated, it was not evident that there was going to be a dramatic cost reduction in simple microprocessor memory. Recent history has shown that the cost of memories may drop sufficiently to allow them to replace film as a simple low cost reconstruction medium.

The major assertions of this present task have been verified. Namely, that a simple mechanical scanner and straightforward arithmetic means can be used to generate a less than perfect, but low cost and usable tomogram. Furthermore, this arithmetically constructed tomogram compares favorably with reconstructions based on far more extensive algorithms. The suggestion that a discrete element memory can replace photographic film is no retreat from this assertion.

APPENDIX A

RECONSTRUCTION OF THE INTERNAL DENSITY STRUCTURE OF AN OBJECT BY ARITHMETIC OPERATION ON A SET OF ITS PROJECTIONS

There are two well-established computational methods of solving the problem of reconstruction from projections. Both of them are computationally lengthy. What will be described is a third method.

A simplified example of the problem is diagrammed in Figure A-1.

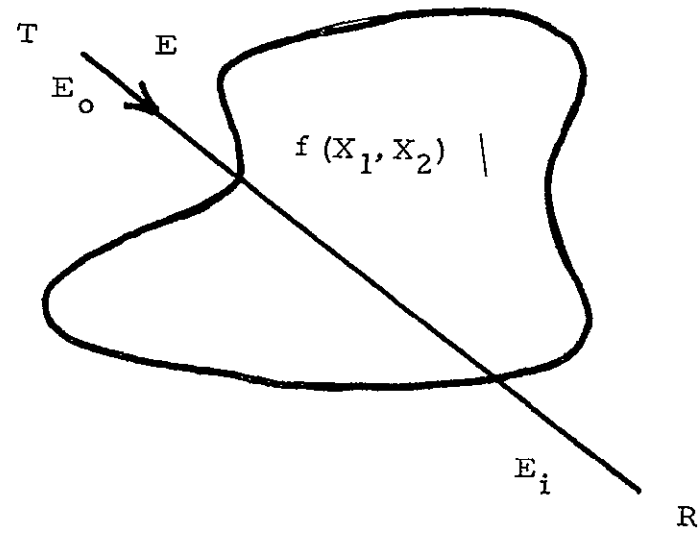

Figure A-1. Test Problem

Some object with a distribution of density throughout space, $f(X_1, X_2)$, is transilluminated by energy E. The transmitting means, T, has a radiation of E_o, but the absorption by f(x) reduces this to E_i by the time it is received by the receiver R.

The problem is to determine the spatial distribution ($f(X_1, X_2 \cdots)$ by an appropriate measure of the possible projections of energy through that distribution.

The arithmetic method for accomplishing this is deceptively simple and is diagrammed in Figure A-2.

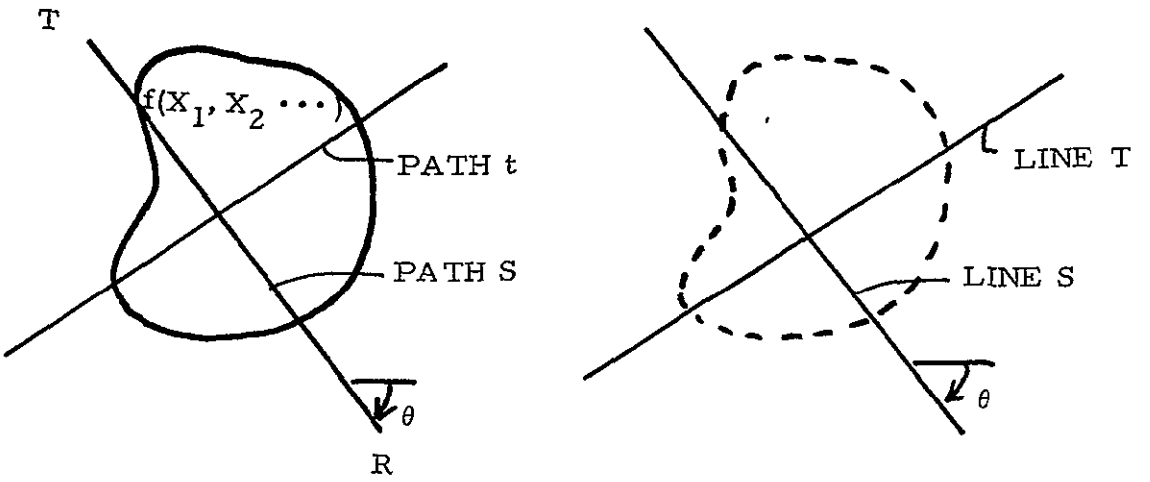

Figure A-2. Initial Reconstruction Logic

The energy received through the object is the integral of the density along some path, S. Establish a reproduction geometry with a line S that is geometrically related to S through the fixed coordinates of the density distribution $f(X_1, X_2 \cdots)$. At each place along S add the numerical value E_i. For every possible transmission path t, establish a reproduction line T and add the value of the line integral along t as a number to every point on the line T. In the limit as all possible views are added, the values on the reproduction plane approach a constant plus a close approximation to the distribution that is desired. It is only necessary to add arithmetically positive values until you are through with the number of projected views, then the constant background level.

Solution Using the Radon Transform

We will be extracting from GEL'FAND (1) for this derivation. While the projection operation is not considered in GEL'FAND's mathematical treatise, it is apparent that the integral of a function over hyperplanes is a generalization of what the scientist measures as a projection.

The functions to be analyzed are infinitely differentiable and rapidly decreasing functions on a real affine space. (For simplicity the function defined on an n-dimensional space will be noted

$$f(X) = f(X_1, X_2 \cdots X_n).$$

The equation of a hyperplane in this space is given by the inner product equality

$$(\xi,X) \equiv \xi_1 X_1 + \xi_2 X_2 + \cdots + \xi_N X_N = p$$

where p is a dimensionless constant.

The volume element is given by the differential form

$$dX = dX_1 \cdots dX_n$$

If a hyperplane of n-1 dimensions is cut through the n-dimensional space, the integral of f(X) over the $(\xi,X) = p$ hyperplane is defined as the Radon transform and is given by

$$\overset{\nu}{f}(\xi,p) = \int f(x)\, \delta\left(p-(\xi X)\right)\, dX$$

where δ ( ) is the impulse "function" and integration is over the whole space.

The Radon transform is thus a function defined on a set of hyperplanes and is an integral operation on the original function.

If, as in Figure A-2, the space is two dimensional, the n-1 dimensional hyperplane is a line S. The integral of $f(X_1 \cdots)$ along that line is a Radon transform of the original function. If the original function represents a density, then the integral of that density is what is measured by the linear projection. In order to provide a physical interpretation of the meaning, consider Figure A-3.

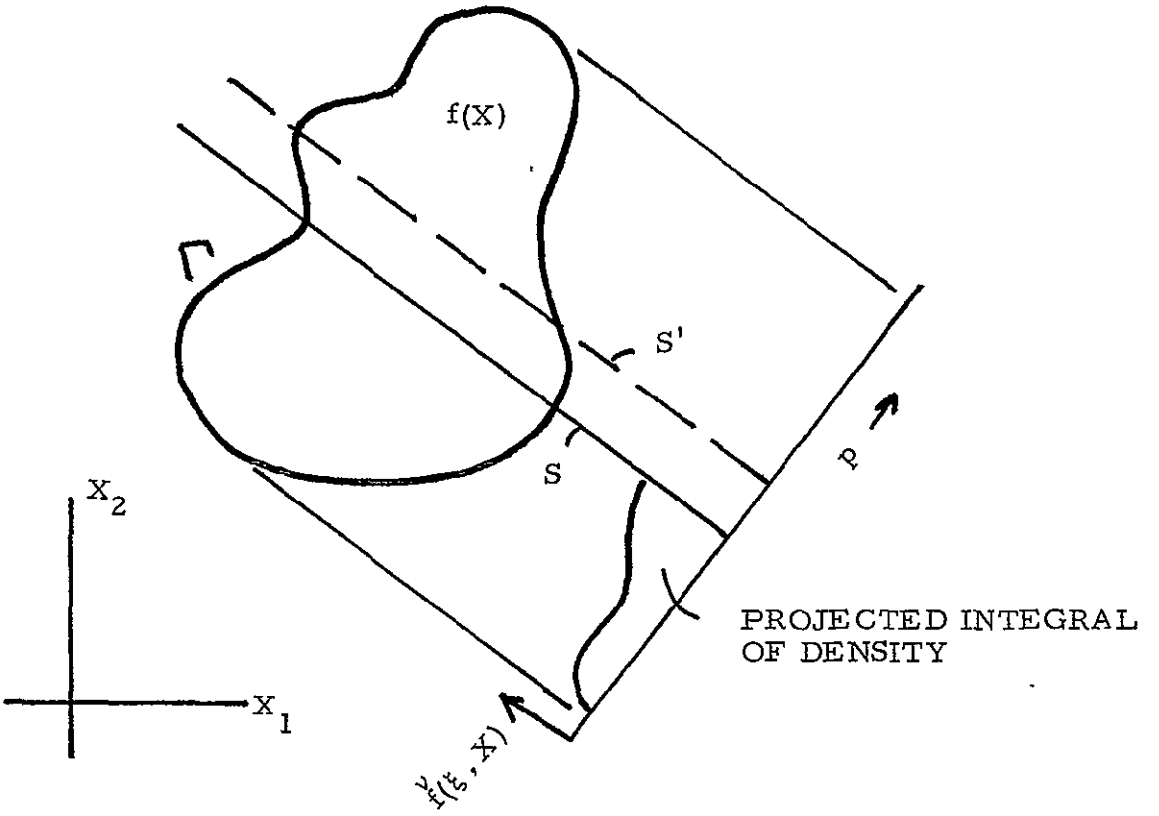

Figure A-3. Projection Correction

The number p designates the numeric of the hyperplane and, in the case of a line, indicates the "parallel location" of that line. This is shown in Figure A-3 by the p-axis drawn perpendicular to the projection line S. Incrementing p to create the new line S' amounts to

a parallel displacement operator. The value of the integral projection at every point p is the Radon transform $\overset{\nu}{f}(\xi,X)$.

The coefficients (ξ_1,ξ_2) for the line

$$\xi_1 X_1 + \xi_2 X_2 = p$$

in Figure A-3 define the "angle" of the line with respect to the X_1,X_2 coordinate. These coefficients have the reciprocal dimensionality of the coordinates X.

The dimensionality relations in the inner product representation for the Radon transform hyperplane is no accident. The Fourier kernel is also defined on an inner product basis and it can be readily shown that there is a close tie between the Radon and Fourier transform. For example, a Fourier transform in n-dimensions reduces to the Radon transform followed by a one-dimensional Fourier transform. In some programs this fact can be computationally advantageous since the Radon transform has the geometrical meaning of an integral projection.

In a real affine space, the inverse Radon transform has a peculiar characteristic that does not exist if a complex space is used, namely, the transform depends upon whether the space is of odd or even dimension.

The types of problem of immediate interest to the reconstruction we are addressing are expressed in two-dimensions, such as Figure A-3.

If the space is two dimensional the inverse Radon transform formula is,

$$f(x) = \frac{-1}{2\pi}\int_{\Gamma} \left[G(\xi)\right]\ \omega(\xi)$$

where,

$$\omega(\xi) = \xi_1 d\xi_2 - \xi_2 d\xi_1$$

and

$$G(\xi) = \int_{-\infty}^{\infty} \frac{\overset{\nu}{f}(\xi,p)}{\{p-(\xi,X)\}^2}\ dp$$

Other than the statement that the value of the inverse transform at some point X depends on the integrals over all possible lines, GEL'FAND drops it there.

Taking a clue from PAPOULIS' (2) discussion of the generalized function t^{-m}, we can proceed as follows. We first find what $G(\xi)$ means in practical terminology. Obviously $G(\xi)$ involves a generalized function, or distribution.

The generalized derivative of the natural logarithm of the absolute value of a coordinate exists and is

$$\frac{1}{p} = \frac{d}{dp} \ell n|p|$$

Thus the integral of $\ln|p|$ with a test function ϕ (p) exists and defines the distribution $\ln|p|$ as,

$$\int_{-\infty}^{\infty} \ell n|p| \, \phi(p) dp$$

It follows then that the generalized derivative of $\ln|p|$ satisfies

$$\int_{-\infty}^{\infty} \frac{\phi(p)}{p} \, dp = - \int_{-\infty}^{\infty} \ell n|p| \phi_p^{(1)}(p) \, dp$$

Continuing, the form for the p^{-m} kernel is

$$\int_{-\infty}^{\infty} \frac{\phi(p)}{p^m} \, dp = \frac{-1}{(m-1)!} \int_{-\infty}^{\infty} \ell n|p| \phi_p{}^{(m)} dp$$

The value of the function G( ) is then tied in with the integral of the second p^{th} derivative of the Radon transform weighted by a logarithmic term.

Consider the geometry shown in Figure A-4.

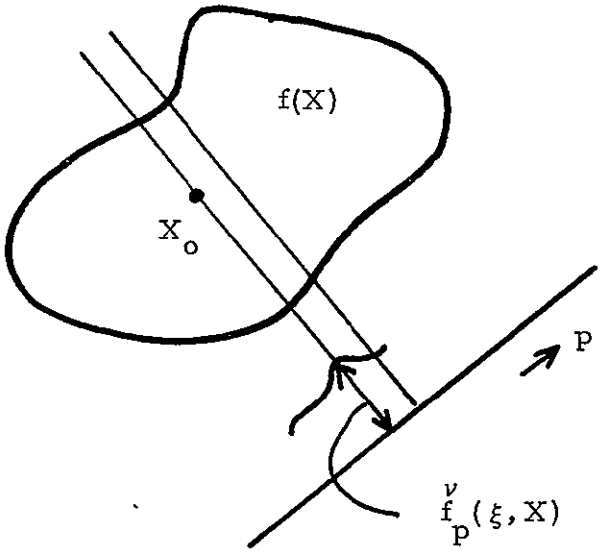

Figure A-4. Definition of Integral

The signal we record as $\overset{\nu}{f}$ is the line integral of the density f(X). The p-axis is the axis perpendicular to our illumination path. The operator

$$\frac{\partial}{\partial p}$$

is the infinitesmal parallel translation operator for the illumination line.

The value of $f(X_o)$ at the line defined by $(\xi,X) = p_o = (\xi,X_o)$ is contained in translation of that line as part of

$$\frac{d}{dp} \overset{\nu}{f} (\xi,X) = f\ (X_o) + \{\text{other } f \text{ along the line}\}$$

The p^{th} second derivative of $\overset{\nu}{f}$ then means,

$$\frac{d^2}{dp^2} \overset{\nu}{f}\ (\xi,X) = \frac{d}{dp} f\ (X_o) + \frac{d}{dp} \{\text{other } f \text{ along the line}\}$$

The term we call G (ξ) then refers to the rate of increment due to $f(X_o)$ as we advance the scanning line along the p-axis. This is not exact, however, because of the $\ln|p|$ weighting term. Now let's take a look at that in Figure A-5.

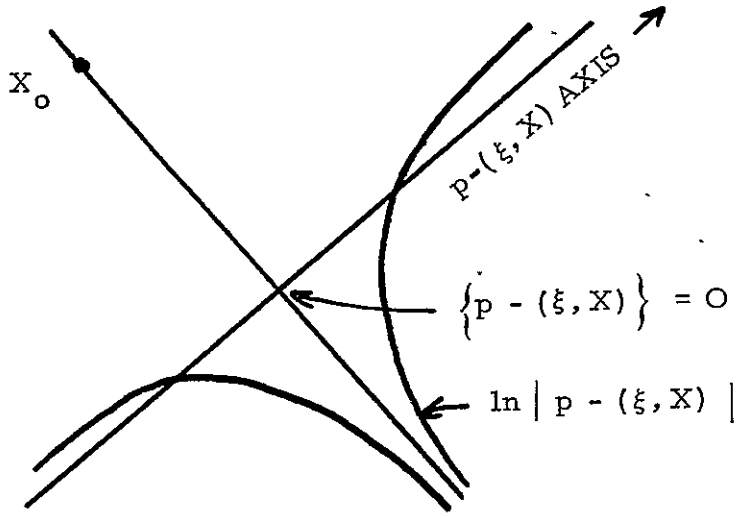

Figure A-5. Effect of Weighting Function

At each point in the object, X_o, we can consider G (ξ) to relate the inversion of the Radon transform as it relates to rays passing through and around X_o but defined by p. In particular the ray passing through X_o is the origin of the p-translation and is where (ξ,X) = p. The weighting function becomes $\ln|p-(\xi,X)|$ and has the shape shown in Figure A-5.

To first approximation the logarithmic singularity "pulls out" the function from inside to outside the integral and "smooths" the values immediately around the coordinate thus extracted. This, coupled with the face that the log of a big number gets big slowly, means we can approximate G (ξ) by

$$G(\xi) \sim \frac{d}{dp} f(X_o) + \frac{d}{dp} \text{ ("smoothed" } f(X_o) + \text{constant}$$

Now the differential $\omega(\xi)$ has an interpretation in ξ -space that can be inferred from Figure A-6.

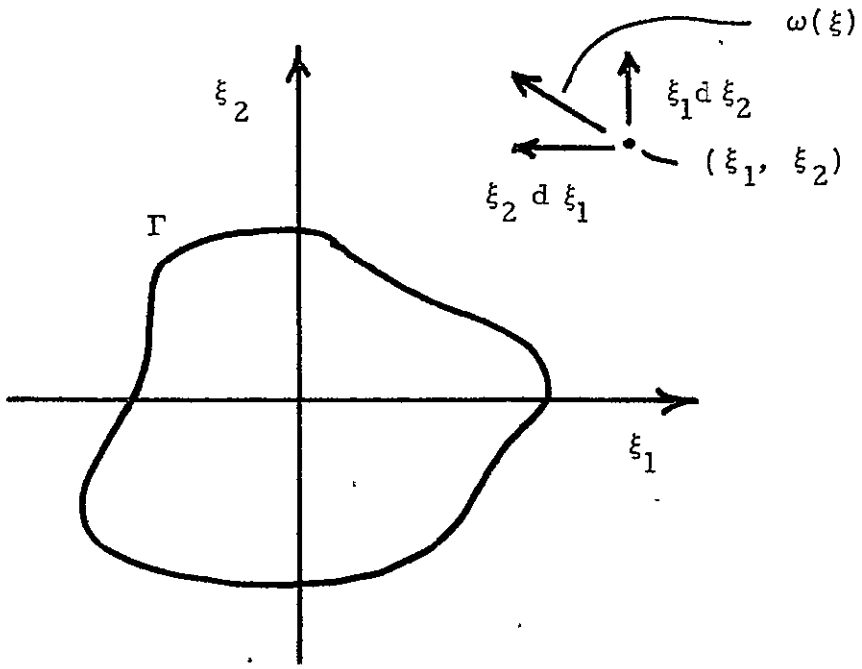

Figure A-6. Description of Coordinate System in ξ-Space

The coefficients, ξ, define the "angle" of the scan line relative to the coordinate axis of $f(x)$. The meaning of $\omega(\xi)$ is the differential for an accumulation along a particular "direction". If we take all possible angles, we accumulate along a closed contour, Γ, which encloses the origin in the ξ -space. In a practical sense we only need accumulate over one half of Γ since the projection of a view taken at 180° and 0° is the same for most physical problems.

The significance of

$$f(X) = \frac{-1}{2\pi} \int_{\Gamma} \left[G(\xi)\right] \cdot \omega(\xi)$$

is that of adding up all possible angular views which pass through X. Taking the first term in our approximation,

$$f(X) \sim \frac{+1}{2\pi} \int \frac{d}{dp} f(X_o)\omega(\xi)$$

we can reconcile the term inside the integral by noting that dp is a parallel translation without angle change. In Figure A-6 we can think of dp as being proportional to $\omega(\xi)$ since a small angle change from one projection to another "adjacent" projection produces a dp change of proportional amount. If you will, the dp of the second projection, considered itself as a projection on the dp of the first, has its orthogonal component (the part not a portion of the first dp) modified as the sine of a very small angle change between the two views.

Thus we can infer that

$$f(X) \sim f(X_o) \quad .$$

In other words, if we take the projection views, and we add them up point by point as we look at all possible view angles, the thing we accumulate has a functional space dependence that is proportional to the original density distribution.

There are two "error" terms which show in this derivation. One is the "smoothed" version of the density and is due to the logarithmic kernel. The other is a constant "background".

The second term is trivial and merely means we must subtract a constant value from each image point.

The first term is more serious and implies we have a slightly out of focus image, since the polarity sign is the same for it as the proper density.

In order to estimate this defocussing, we can return to the generalized derivative of $\ln|p|$

$$\int_{\infty}^{\infty} \frac{\phi(p)}{p}\, dp = -\int_{\infty}^{\infty} \ell n|p|\, \phi_p^{(1)}(p)dp$$

This is a Hilbert transform relationship defined at the p = 0 place. The Hilbert transform of a function g (x) is defined as

$$h(X) = \frac{1}{\pi} P \int \frac{g(y)}{y-x} \, dy$$

where P means the Cauchy principal value is to be used (pre-generalized function notation). We can get a reasonable idea of the smoothing effect of $\ln|p|$ by noting how the Hilbert transform of a function differs from the derivative of that function.

Obviously the smoothing effect on an impulse is r^{-1} where r is the radial distance away from the coordinate of the impulse. Discrete image points are not impulses, however, they are more like Kronecker deltas with finite height. The smoothing effect in that case is very small. Other examples, such as edge transitions can be likewise examined.

In summary, the method of arithmetic reconstruction appears analytically valid and offers a simple solution.

Heuristic Argument in Signal Space

One can offer a reasonable explantion as to why arithmetic reconstruction works. Consider Figure A-7.

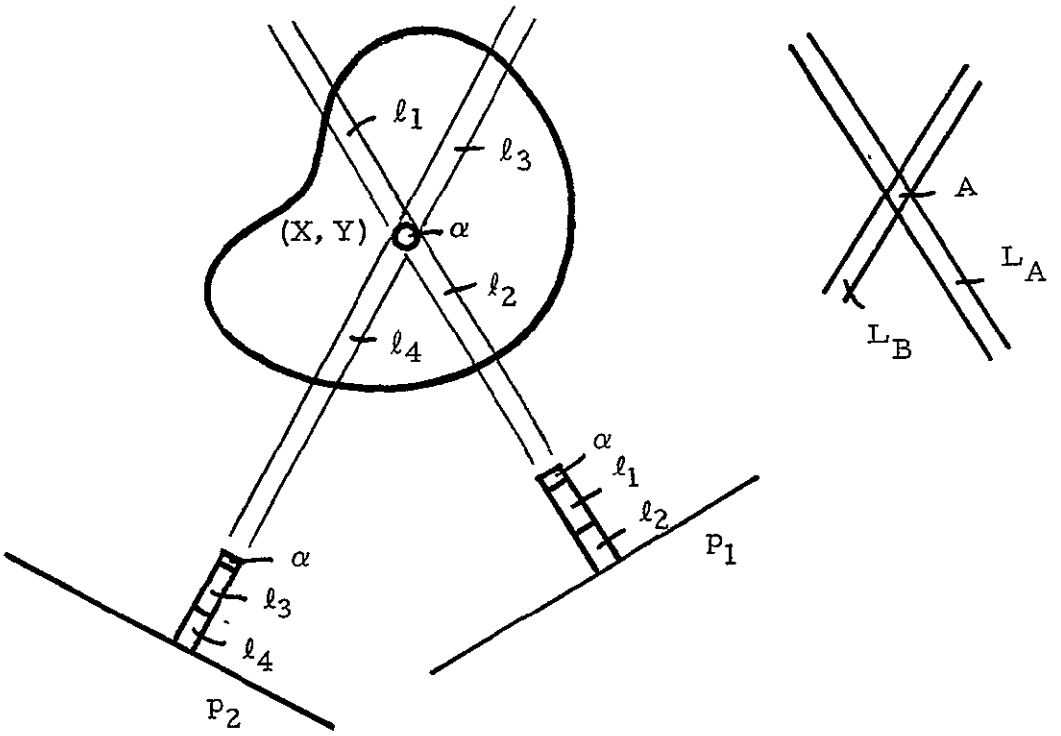

Figure A-7. Arithmetic Reconstruction

The projection, p_1, through some point (X, Y) has a portion of its density change, α, due to that point. The integral of the density has two terms: ℓ, due to the line integral of everything along the path except α, and α itself.

If lines L_A, L_B, etc. were laid down on a reproducing plane in direct geometric relation to the recording projection lines, and if the density of values along the L's were equal to the projection integral, the net density at the point A, corresponding to the real α, becomes

$$(\ell_1 + \ell_2 + \alpha) + (\ell_3 + \ell_4 + \alpha) + \ldots + (\ell_{2n-1} + \ell_{2n} + \alpha)$$

The total area of the original density, calculated from rays drawn from α is

$$\text{AREA} = \ell_1 + \ell_2 + \ell_3 + \ell_4 + \cdots + \ell_{2n-1} + \ell_{2n} + \alpha$$

In the area computed from a finite number of rays originating at α, each ray is added and α is itself only added once. In the reconstruction from projection integrals the net value at α is made up of the sum of the rays plus N-times the sum of α. Consequently the net density at each point (X, Y) is

$$D(X,Y) = \text{AREA} + (N-1)\ f(X,Y) + (N-1)\ (\text{smoothed } f(X,Y))$$

where f(X,Y) is the original density distribution. This is exactly what we predicted from the inversion of the Radon transform. The smoothed term comes about because we assumed a finite projection width in Figure A-7. The "star" patterns of converging rays overlap very close to (X,Y) and cause a small amount of defocussing. The "area" term is the constant background that must be removed.

The amount of smoothing is due to the finite resolution of a practical system of making projections. It is in fact the amount of edge smoothing we will see in any single projection image. If the line width of projection becomes vanishingly small, the smoothing term will be reduced similarly when a finite number of projections is used. Apparently, the use of an infinite number of projections will again lead to a small amount of smoothing. What appears to be happening with a finite number of infinitely narrow width projections is that the term we call "area" cannot be the true area because there are density portions missed between the "spokes". The fluctuation of this "area" as a function of (X,Y) is where the smoothing occurs in this case.

Argument in Fourier Space

There is yet another way of looking at the method of arithmetic reconstruction. The Fourier transform of a projection is the corresponding slice of the two dimensional Fourier transform of the complete object. See Figure A-8.

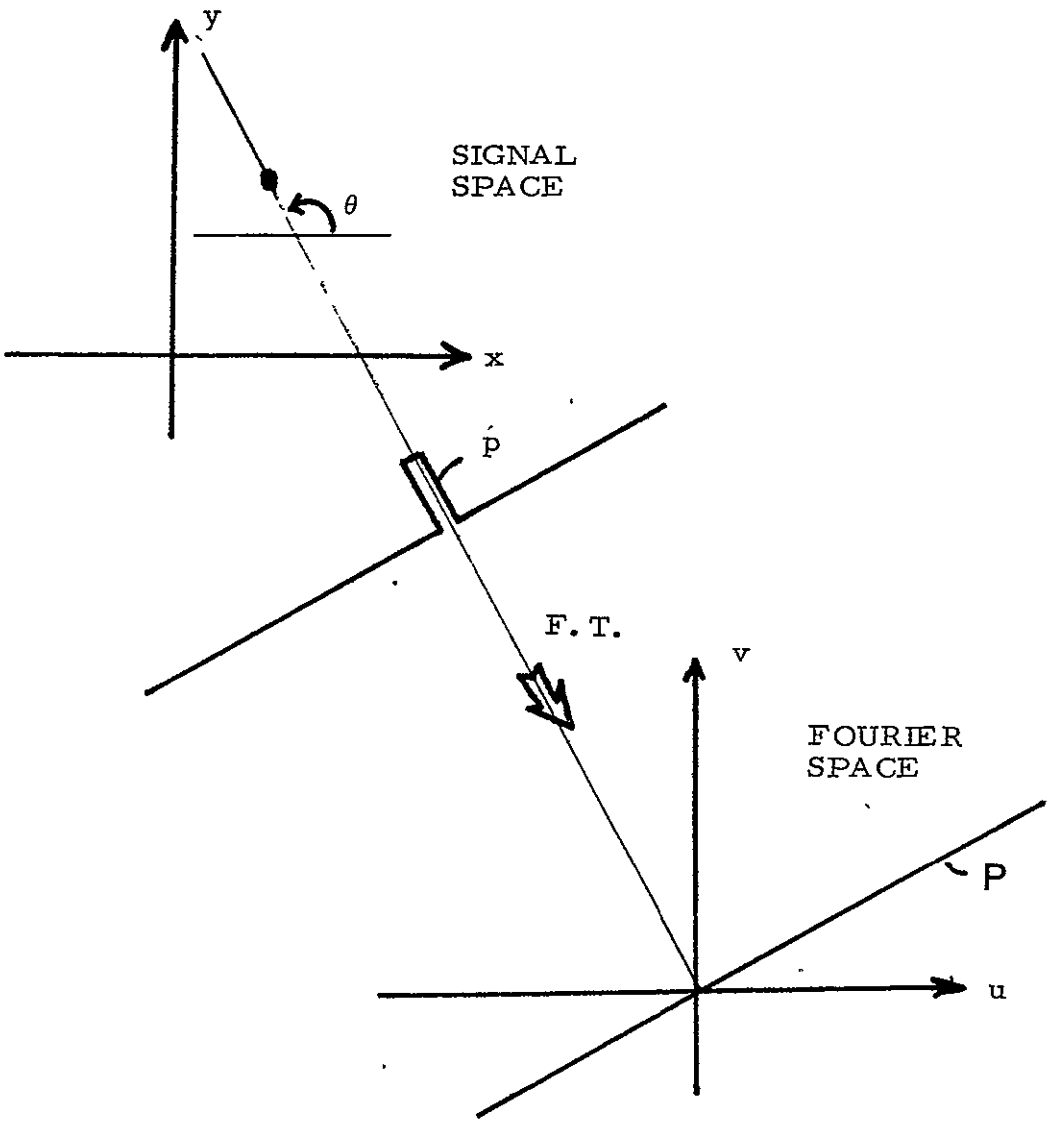

$$P(u, v) = \iint p(x, y) e^{i2\pi(xu+yv)} dxdy$$

Figure A-8. Reconstruction in Fourier Space

If a number of projection views are taken at different angles, the two dimensional Fourier transform is approximated as shown in Figure 9.

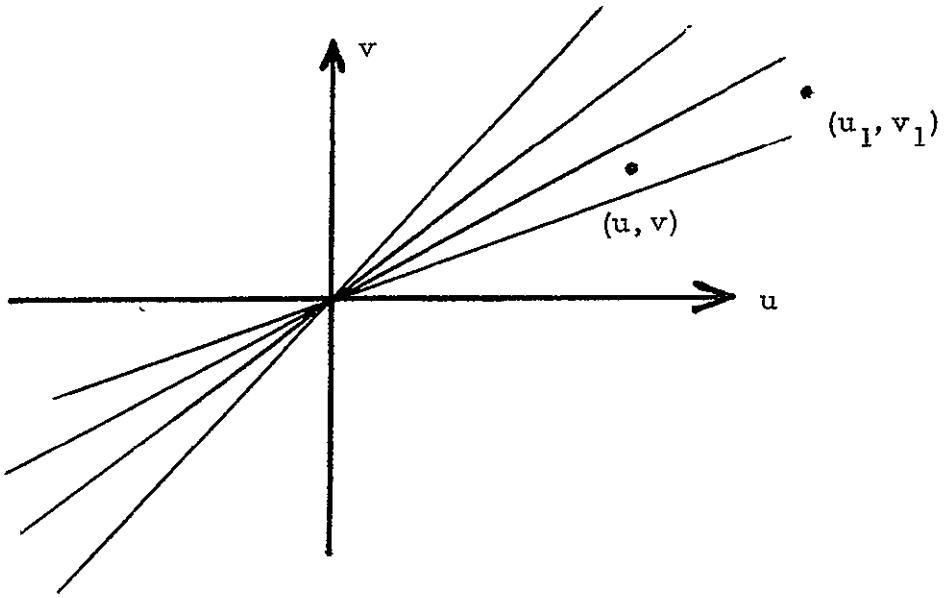

Figure A-9. Fourier Test Case

The Fourier transform is not only two dimensional but complex, having a magnitude and phase angle as a function of spatial frequency. Points, such as (u,v), which lie between the Fourier "spokes" may be approximated by extrapolation to those known projection transforms which are nearest. As one passes farther out in frequency, such as to point (u_1,v_1), the approximations become less accurate per unit increment of spatial frequency.

All Fourier slices pass through the origin. This "overspecification" means that the reconstructed image made from a straight summation of slices will have a large zero frequency component.

The lack of inter-spoke preciseness may be interpreted as giving a high frequency smoothing. If we simply arithmetically add up all the inverse Fourier transforms of this pattern we can expect the resultant to be

$$F(X,Y) + \text{smoothed } f(X,Y) + \text{constant}$$

Again, this is exactly what we expect.

References

(1) I. M. GEL'FAND, M. I. GRAEV, and N. YA VELENKIN, Generalized Functions, Vol. 5, Integral Geometry and Represenation Theory (Academic Press, N.Y., 1966).

(2) A. PAPOULIS, The Fourier Integral and its Applications (McGraw-Hill Book Co., N.Y., 1962).

Appendix B

Reconstruction in the Presence of Boundary Reflections

Sound energy will be diminished when passing through a boundary separating regions of differing acoustic impedance. Thus, even if the regions through which the sound passes have no inherent absorption of acoustic energy, there will be a reduction in transilluminated sound. This raises the question whether a reconstruction of internal density structure from integral projections will be adversely affected by such boundaries.

The presence of such boundary conditions will not, to first order, detract from the reconstruction. Consider the idealized case shown below. A generalized boundary, B, separates a medium with acoustic impedance Z_1 from a medium with acoustic impedance Z_2. The boundary is assumed to be very thin, since it represents a transition in acoustic impedance.

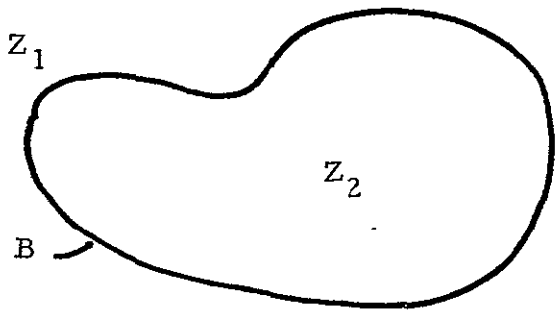

Fig. 1

This boundary can be considered a continuous locus of scattering point centers, much like a densely packed string of very small beads. In forming all possible views by sets of projections, each point on the boundary will act as a point scatterer independent of all other boundary points. In effect the boundary is made up of a contiguous set of point scatterers, each of which contributes a constant reduction of passing sound energy. The area within the boundary will therefore be reconstructed with an indication of a slightly higher average density than would be the case had the boundary not been present.

If linear reconstruction methods are used, then each point scatterer will appear in its proper geometric place, have the proper value of indicated attenuation, and be out of focus by the same amount due to the finiteness of transilluminated beam. This means that the boundary will appear in its proper place.

If the region within the boundary has an additional attenuation which represents a different density structure than the region outside the boundary, the reconstruction will proceed unmodified by the fact that there is a boundary. This is because the sound wave is diminished by a constant value, representing the boundary point.

Appendix C

Program Used for Computer Simulation


```
FORTRAN IV-PLUS V01-03          09 22 48    20-SEP-77          PAGE 1
CAT125 FTN      /TR BLOCKS

0001            DIMENSION CARG(24),SARG(24)
0002            INTEGER*2 DTX(26,150),ODN,SPAR(5)
0003            BYTE DT(100,100),A(5176),LABEL(512)
0004            DATA LABEL/70*32,'S','C',70*32,'A','L',368*32/
0005            ODN=1+IUNIT(5)
0006            CALL PARAM(NP,ODN,1,,' ENTER OUTPUT DDD ')
0007     2      FORMAT(1H ,65I2)
0008            CALL MVL('CAT OUTPUT PICTURE',LABEL(74),18)
0009            NT=1
0010            DO 35 N=1,100
0011            DO 35 M=1,100
0012    35      DT(N,M)=0
0013            DO 34 N=24
0014            DO 34 M=1,150
0015    34      DTX(N,M)=0
0016            DO 400 NROT=1,24
0017            ARG=(NROT-1)*3 14159/24
0018            CARG(NROT)=COS(ARG)
0019     400       SARG(NROT)=SIN(ARG)
0020            DO 1 N=1,100
0021            DO 1 M=1,100
0022            IVW=(N-50)**2+(M-50)**2
0023            IF((IVW LT 155) AND.(IVW.GT.56))DT(N,M)=8
0024            IVX=(N-30)**2+(M-50)**2
0025            IF(IVX LT 25)DT(N,M)=9
0026            IVR=(N-69)**2+(M-50)**2
0027            IF(IVR LT 25)DT(N,M)=9
0028            IVQ=(N-50)**2+(M-68)**2
0029            IF(IVQ.LT 25)DT(N,M)=9
0030     1      CONTINUE
0031            CALL  PARAM(NP,NTEST,1,,' TYPE 3   ENHANCE,2OR  3 GEN,OR 1 ')
      C GENERATE PROJECTIONS
0032            DO 500 N=2,99
0033            DO 500 M=2,99
0034            I=M+1
0035            J=M-1
0036            K=N+1
0037            L=N-1
0038    500     DT(J,L)= 4*DT(M,N)+ 1*(IV(DT(M,K))+IV(DT(M,L))+IV(DT(1,N))+
              1 IV(DT(J,N)))+ 05*(IV(DT(I,K))+IV(DT(I,L))+IV(DT(J,K))+
              2  IV(DT(J,L)))
0039            DO 5011 M= 2,99
0040            DO 5011 N=2,99
0041            J=101-N
0042            JJ=100-N
0043            K=101-M
0044            L=100-M
0045     5011   DT(K,J)=DT(L,JJ)
0046            IF(NTEST EQ 1)GOTO1000
0047            DO 25 NROT=1,24
0048            DO 25 NINC=1,120
0049            DO 4 NNINC=1,120
0050            N=-(NNINC-50)*SARG(NROT)+50.5+(NINC-50)*CARG(NROT)
0051            M=(NINC-50)*SARG(NROT)+50 5+(NNINC-50)*CARG(NROT)
0052            IF(((M GT.99) OR.(M LT 2)) OR ((N.GT 99).OR (N.LT 2)))GOTO4
0053            DTX(NROT,NINC)=DTX(NROT,NINC)+DT(N,M)
```

```
FORTRAN IV-PLUS V01-03          09 22.48    20-SEP-77          PAGE 2
CAT125 FTN      /TR:BLOCKS

0054      4     CONTINUE
0055     25      CONTINUE
0056             DO 42 N=1,120
0057             DTX(25,N)=0
0058             DO41 M=1,24
0059     41      DTX(25,N)=DTX(M,N)+DTX(25,N)
0060     42      DTX(25,N)=DTX(25,N)/24
0061             PRINT 30
0062             DO 5 N =1,25
0063             PRINT 28,N
0064     28      FORMAT(1H ,I2)
0065     5       PRINT 27,(DTX(N,M),M=1,120)
0066     27      FORMAT (1H ,30I4)
         C ENHANCE PROJECTION
0067             IF(NTEST.EQ.2)GOTO17
0068             DO 200 N=1,24
0069             DO 201 M=2,149
0070             L=M-1
0071             K=M+1
0072      201    DTX(26,M)=3 4*DTX(N,M)-1 2*(DTX(N,L)+DTX(N,K))
0073             DO 200 M=1,150
0074      200    DTX(N,M)=DTX(26,M)
0075             PRINT 30
0076      30     FORMAT(1H )
0077             DO 501 N=1,25
0078             PRINT 28,N
0079      501    PRINT 27,(DTX(N,M),M=1,120)
         C  REPROJECT BACK
0080     17      DO 7 N=1,100
0081             DO 7 M=1,100
0082       7        DT(N,M)=0
0083             DO 8 N=1,100
0084             DO 8 M =1,100
0085             DTQ=0
0086             DO 81 NROT = 1,24
0087             NINC= 50+(N-50 5)*CARG(NROT)+(M-50.5)*SARG(NROT)
0088             IF((NINC LT 1) OR (NINC.GT 150))GOTO81
0089              DTQ=DTQ+DTX(NROT,NINC)
0090     81      CONTINUE
0091       8         DT(N,M)=DTQ/100
0092             PRINT 30
0093     1000    DO 100 N=1,100
0094       100      PRINT 2,(DT(N,M),M=20,84)
0095             CONTINUE
0096             CALL OPEN(A,2560,1,1,ODN)
0097             SPAR(1)=100
0098             SPAR(2)=100
0099             SPAR(3)=8
0100             SPAR(4)=4
0101             SPAR(5)=512
0102             CALL PLABEL(A,SPAR,LABEL)
0103             DO 150 I=1,100
0104             CALL PUT(A,0,IA)
0105      150    CALL MVL(DT(1,I),A(IA+1),100)
0106             CALL CLOSE(A)
0107             END
```